Revised manuscript (clean version)

Numerical Simulation with a Macroscopic CFD Method and Experimental Analysis of Wave Interaction with Fixed Porous Cylinder Structures

Dongsheng Qiao[1], Ed Mackay[2], Jun Yan[1*], Changlong Feng[1,3],
Binbin Li[4], Anna Feichtner[2], Dezhi Ning[1**], Lars Johanning[2]

1. State Key Laboratory of Coastal and Offshore Engineering, Dalian University of Technology, Dalian 116024, China;
2. Renewable Energy Group, CEMPS, University of Exeter, Penryn Campus, Penryn, Cornwall TR10 9FE, UK;
3. CCCC Water Transportation Consultants Co. Ltd. Qingdao Branch, Qingdao 266071, China;
4. Shenzhen International Graduate School, Tsinghua University, Shenzhen 518055, China.

Abstract:

Porous structures have been widely applied in the coastal and ocean engineering due to their wave energy dissipation mechanism. The macroscopic computational fluid dynamics (CFD) approach where the quadratic pressure drop condition of porous surface is introduced to model the wave interaction with porous cylinders. A series of CFD simulations of waves interacting with a single porous cylinder and the combined structure of a porous cylinder with a concentric inner solid column are performed, with corresponding tank tests conducted. The CFD method is compared with experiments, linear potential model, and the quadratic BEM (boundary element method) model. The effects of porosity and porous cylinder radius on wave force and wave heights inside porous cylinder are analyzed to evaluate the performance of porous shell reducing wave loads and wave surface elevation, and the wave force variation with incident wave amplitudes are also investigated. The results demonstrate that the established CFD model is reliable for engineering analysis and thereby being of great significance for reference purpose in the CFD simulations of waves interacting with porous structures.

Keywords: Porous cylinder; Wave-structure interaction; Model tests; Macroscopic CFD method; Quadratic pressure drop

1 Introduction

The cylindrical structures are widely used in offshore engineering as support structures, such as the offshore oil platforms, the offshore wind turbines and the bridge foundations. These cylinders are usually partly submerged below the water surface, and mainly impacted by wave loads. If the wave force and the wave run-up caused by external wave loads become too large, the safety of whole structure will be threatened. So far, many studies have been carried out for the wave force and wave run-up on the cylindrical structures by numerical or experimental methods (Bonakdar et al., 2016; Mohseni et al., 2018; Chen et al., 2020; Ha et al., 2020), on the other hand, mitigation of wave loads for such cylindrical structures is also worth to be considering.

* Corresponding author. Email address: junyan@dlut.edu.cn;
** Corresponding author. Email address: dzning@dlut.edu.cn.

Due to the ability to enhance their wave energy dissipation and reduce the wave heights around structures, porous structures have been widely used for absorbing wave impact and protecting structures in the coastal and ocean engineering. Examples are submerged porous breakwaters (Liu et al., 2012), fixed permeable caisson breakwaters (Huang et al., 2011), wave absorbing chambers of floating offshore base (Liu et al., 2013), and the porous collar barrier for offshore floating fish cage (Chu and Wang, 2020). There are a large number of studies focused on wave interaction with porous structures. Some studies conducted the physical model tests in wave tanks, to investigate the hydrodynamic performance of porous structures. For example, Tabet-Aoul and Lambert (2003) conducted a series of tank tests and investigated the point pressure and total horizontal wave force on the porous structures with different porous plates; Metallinos et al. (2016) investigated the wave propagation of a submerged porous breakwater on a steep slope in a physical model test; Francis et al. (2020) analyzed the effect of porosity on the wave energy dissipation by conducting an experimental test on solitary wave interacting with the vertical porous plates. Christensen et al (2016) conducted an experimental study of floating breakwaters, and analyzed the effect of two different damping mechanisms of a floating breakwater. The wave interaction with a perforated square caisson and a vertical cylinder encircled by a perforated square caisson are studied by Neelamani et al. (2000, 2002) through a series of tank tests, and the effects of caisson porosity, incident wave height and wavelength on the wave force and wave surface fluctuations are analyzed. Vijayalakshmi et al. (2007a, 2007b) further investigated the wave interaction with a perforated circular caisson and a concentric twin perforated circular cylinder.

Given that tank tests are limited by experimental conditions, many researchers developed mathematical models for wave interaction with porous structures, which are usually conducted based on potential flow theory. Sollitt and Cross (1972) modeled porous media as a homogeneous surface and proposed that the flow through the porous surface was subjected to a pressure drop. The pressure drop across the porous surface is a function of flow velocity and acceleration, where the velocity terms account for the energy dissipation across the porous surface, which is deemed to be proportional to the square of the velocity for thin porous barriers; the acceleration terms represent inertial effects, which is caused by the acceleration of flow through the openings. Based on this model, Chwang (1983) and Yu (1995) assumed that the energy dissipation was linear in the velocity and proposed a ‘porous-effect parameter’ to represent the linearized pressure drop across the porous surface, to simplify make the analysis for wave interaction with porous structures. A large number of studies on wave interaction with porous structures were conducted flowing this linearized pressure drop assumption. Suh et al. (2006) and Liu et al. (2008a, 2008b) conducted the analytical investigations on wave interacting with perforated wall caissons with linear pressure loss assumption and validated the analytical models with experiments. Geng et al. (2018) adopted a similar method to study the influence of the thickness, the porosity and the layout of plates on the wave absorptivity of vertical porous plates.

In addition to vertical porous wall or plate, there are also many investigations adopting the linear pressure loss assumption to analyze the wave interaction with porous cylindrical structures. Liu et al. (2013, 2018a) analyzed the wave diffraction of two and multiple concentric porous cylinders by using the eigenfunction method. Wave loads on a bottom-fixed cylinder surrounded with porous outer cylinders of different forms were analyzed under linear waves (Wang and Ren, 1994; Wu and Chwang, 2002; Cong and Liu, 2020), solitary waves (Zhong and Wang, 2006) and short-crested waves (Gao and Li, 2012; Song and Tao, 2007). Similar investigations were conducted on various types of floating or truncated porous cylinders (Williams et al., 2000; Zheng et al., 2005; Ning et al., 2016). Sankarbabu et al. (2007, 2008) and Weng et al. (2016) considered the wave forces on different arrays of porous cylinders. Liu et al. (2018b) derived the solution of regular wave interaction with a concentric porous cylinder system, which has an arbitrary smooth section. Although the linear pressure drop assumption adopted in above investigations enables analytic and semi-analytic solutions to be derived, it still has limitation for engineering application. In the linear pressure drop assumption, the dissipation coefficient in 'porous-effect parameter' is depended on the geometrical parameters of particular porous structures and wave conditions, and is usually obtained from experiments, which causes inconvenience for engineering application. Furthermore, the linear model cannot well predict the nonlinear variation of wave forces with wave amplitude.

There are also some models established with quadratic pressure drop condition, where the coefficients in pressure drop are only depended on the properties of the porous material and not the geometry of the structure as a whole. Most of them are proposed for fixed porous barriers in 2-dimension (2D). Bennett et al. (1992) adopted the quadratic pressure drop to calculate the reflection properties of slotted wave screen breakwaters, and given the results for screens both with and without a solid backing wall and comparisons with experiment show excellent agreement. Molin and Fourest (1992) proposed an analytical solution for wave refection by a fully perforated caisson breakwater with multi chambers, by solving the quadratic pressure drop condition. Zhu and Chwang (2001) similarly developed an analytical solution for wave reflection by a semi-immersed perforated thin wall with an impermeable rear wall. Liu and Li (2017) proposed a multi-domain BEM method with quadratic pressure drop condition and recommended the suitable values of discharge coefficient and blockage coefficient in the quadratic pressure drop condition for perforated caissons. The comparison with experimental data in previous studies shown good agreement of the nonlinear variation of forces and reflected waves with wave heights. Mackay et al. (2019) proposed a similar BEM model for thin porous plates and compared the results to the physical model tests. In addition, there are some models conducted with quadratic pressure drop condition for porous cylinders in 3-dimension (3D). Dokken et al. (2017) proposed a BEM model with a quadratic pressure drop, to solve the wave radiation and diffraction problems of a floating porous cylinder. An extended BEM model for wave interaction with thin porous elements is proposed by Mackay et al. (2021), and the wave interaction with bottom-fixed and floating porous cylinders are investigated (Mackay et al., 2020).

The quadratic pressure drop condition can more accurately reflect the pressure-velocity relationship on the porous surface, and the application for engineering practice is more feasible since the coefficient depend only on the properties of the porous material. However, in wave-structure interaction, the viscous effects also need to be considered, which is not possible in linear potential flow models. For this circumstance, a CFD method can be adopted, which also has the advantage of capturing the variation of wave surface elevations. Chen et al. (2019) used Ansys Fluent to create a 2D numerical wave tank (NWT) and performed simulations on the interaction between waves and a vertical porous wall placed in solid wall front. Ren and Ma (2015) used the CFD method to establish a 3D NWT and simulated the interaction between nonlinear waves and perforated quasi-ellipse caissons. A detailed CFD model with microstructural geometry is feasible for porous structures. However, this requires a very fine mesh to properly resolve the flow through the openings in the porous material, which results in high computational times. An alternative CFD method is using a volume-averaged macro-scale model to represent the impact of porous structure on the flow, by means of applying a pressure-drop as a momentum source in a geometrically defined porous-media zone. The macroscopic CFD method has been applied for wave interaction with rubble mound breakwaters and dams (Liu et al.,1999; del Jesus et al., 2012; Higuera et al, 2014; Jensen et al, 2014; Molines et al., 2020), and thin porous structures such as fish nets and cages (Shim et al.,2009; Zhao et al., 2014; Chen and Christensen, 2016) and perforated sheets (Feichtner et al., 2020). The macroscopic method avoids the complex mesh generation and thus significantly reduces computational efforts, which is meaningful for engineering application where large-scale effects are of the main interest.

The motivation for the present study is to validate the reliability of macroscopic CFD method, linear potential model, and the quadratic BEM model for replicate wave force and free surface elevation of wave-porous cylinder interaction, and to investigate the potential of porous shells for reducing loads on fixed offshore structures and wave heights around them. In previous studies (Feitchtner et al, 2019; Qiao et al., 2020), a macroscopic CFD model was established with quadratic pressure drop condition adopted for simulating the wave interaction with thin porous plate, and the comparison with experimental results shown that the alternative CFD method is feasible. In present study, an extended macroscopic CFD model is established for wave interaction with bottom-fixed cylinders. The established CFD model is firstly applied to a single porous cylinder shell, with the wave force on it and the wave elevation inside the cylinder being analyzed. Then a porous cylinder shell with a solid inner cylinder is considered. The analysis of the nonlinearly variation of wave force and wave elevation inside cylinders with the incident wave heights is also considered. In addition, a series of model tank tests is conducted to compare the results of CFD, linear potential flow solution and quadratic BEM model.

The organization of this paper is as follows. The experimental setup is presented in Section 2. Section 3 presents the establishment of macroscopic CFD model. The analysis on a single porous cylinder shell and a porous cylinder shell with an inner solid cylinder is respectively presented in Section 4 and 5. The variation of wave force with the incident wave heights is discussed in Section 6. The conclusions are presented in Section 7.

2 Experimental setup

In this study, a series of model tank tests were conducted to observe the characteristics of wave interaction with a fixed porous cylinder with and without an inner solid cylinder. The tank tests were conducted in the 2D wave flume at Dalian University of Technology (DUT). The length of flume is 60 m, the width is 4.0 m, and the working water depth is 0.2 m–2.0 m. The flume has a hydraulic servo push-plate wave making system, which can produce regular and irregular waves, with the wave period ranging 0.5s-5.0s. Figure 1 shows the cylinder models used in the tests. The solid cylinder is made from PMMA with a height of 1.5m and a diameter of 0.25m. The porous cylinders are made from aluminum porous plates with 5mm width by rolling up and welding, with a cap on the top. The total height of the outer porous cylinder is 1.7m, including a porous area of 1.5m height, and the diameters are 0.375m, 0.5m and 0.75m, respectively. The distance between the outer porous cylinder and the tank wall is at least three times of the cylinder diameter, which is deemed wide enough to avoid the influence of boundary effects. The porous cylinders (plates) have circular holes arranged in a regular grid pattern, with hole radius r and interval s, as shown in Figure 2. In this experiment, the interval s is set as 25mm, and the radius r is changed with the porosity of outer cylinder being 0.1, 0.2 and 0.3. The porosity ε is defined as the ratio of the area of openings to the total porous surface area of cylinder, which is calculated as:

$$\varepsilon = \pi r^2 / s^2 \tag{1}$$

The outer porous cylinder and the inner solid cylinder are connected by a bolt in the top side, and in the bottom side, they are fixed to a disk, as Figure 3 shown. Two load cells are respectively installed on the cap of outer porous cylinder and the bottom disk, to monitor the wave force on the combined structure, in which the lower load cell is located in a small pit beneath the tank floor to enable the experimental model being close enough to the tank floor, as shown in Figure 4. The adopted load cells can measure forces in three orthogonal directions, with an accuracy of 0.01N, maximum range of ± 400N in X/Y direction and ± 2250N in Z direction, nonlinearity <0.5%, repeatability <0.3%. A temporary raised section of floor was installed in the section of the flume where the model is installed. Figure 5 shows the wave probes applied in this experiment. There are five wave probes placed in front of and behind the model to monitor the wave surface elevations. Figure 6 shows the synchronous acquisition system. The signals from load cells and wave probes are sent to their corresponding amplifiers and then collected by the data acquisition card controlled by a computer. This allows for synchronization between wave surface elevations and wave force in monitoring. The data acquisition speed in experiments is 100Hz. The schematic of experimental setup in DUT wave flume is shown in Figure 7. The experimental water depth is 1.0m. A series of regular wave conditions with the normalized wave number kd ranging 0.6~3.4 and the wave steepness kA ranging 0.05~0.20 are applied in the tests. Before the model tests, empty water tank tests are conducted to correct the wave-making system to ensure that the required wave conditions can be generated, and there is no breaking effect observed under the steepest wave.

(a) Inner solid cylinder (b) Outer porous cylinder

Figure 1 Experimental cylinder models

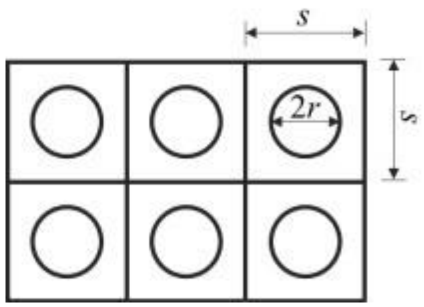

Figure 2 Illustration of regular grid of holes in porous cylinders (plates)

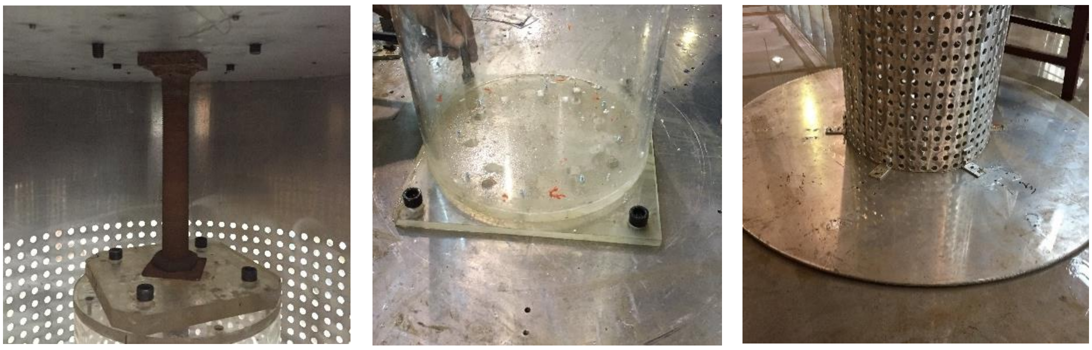

Figure 3 Connection of inner and outer cylinders

(a) Top load cell (b) Bottom load cell

Figure 4 Load cells and their installation

Figure 5 Wave probes installation

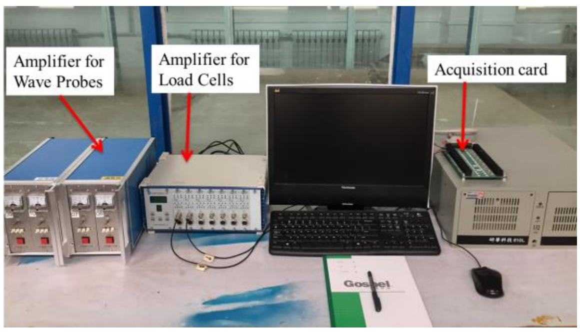

Figure 6 Synchronous acquisition system

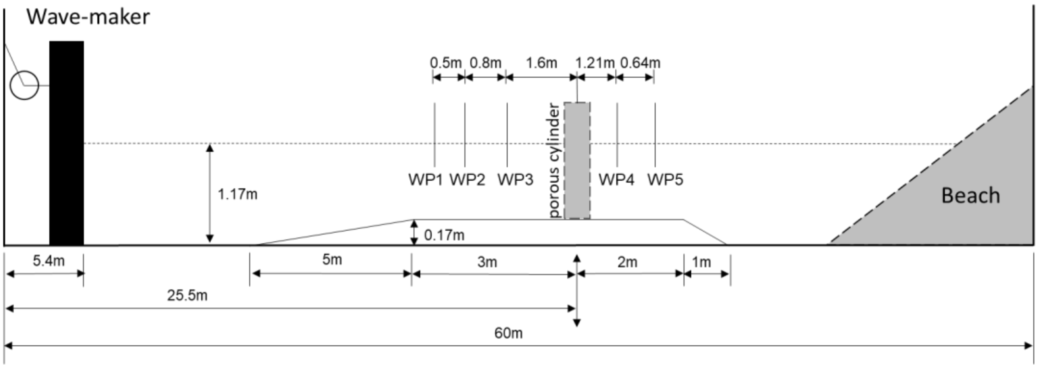

Figure 7 Schematic of experimental setup in DUT wave flume

3 CFD method

3.1 Numerical wave tank

The Navier-Stokes equations of general form are used to describe the flow in NWT:

$$\frac{\partial u}{\partial x}+\frac{\partial v}{\partial y}+\frac{\partial w}{\partial z}=0 \tag{2a}$$

$$\frac{\partial u}{\partial t}+u\frac{\partial u}{\partial x}+v\frac{\partial u}{\partial y}+w\frac{\partial u}{\partial z}=-\frac{1}{\rho}\frac{\partial p}{\partial x}+v\left(\frac{\partial^2 u}{\partial x^2}+\frac{\partial^2 u}{\partial y^2}+\frac{\partial^2 u}{\partial z^2}\right) \tag{2b}$$

$$\frac{\partial v}{\partial t}+u\frac{\partial v}{\partial x}+v\frac{\partial v}{\partial y}+w\frac{\partial v}{\partial z}=-\frac{1}{\rho}\frac{\partial p}{\partial y}+v\left(\frac{\partial^2 v}{\partial x^2}+\frac{\partial^2 v}{\partial y^2}+\frac{\partial^2 v}{\partial z^2}\right) \tag{2c}$$

$$\frac{\partial w}{\partial t}+u\frac{\partial w}{\partial x}+v\frac{\partial w}{\partial y}+w\frac{\partial w}{\partial z}=-\frac{1}{\rho}\frac{\partial p}{\partial z}+v\left(\frac{\partial^2 w}{\partial x^2}+\frac{\partial^2 w}{\partial y^2}+\frac{\partial^2 w}{\partial z^2}\right)-g \tag{2d}$$

where, u , v and w are the instantaneous velocity in three directions; ρ is the density of water; p represents the instantaneous effective pressure; υ is the molecular viscosity, g is the acceleration of gravity. The free water surface in NWT is captured by the volume of fluid (VOF) method, and for each control volume, the volume fraction of air and water phases fit the following equations:

$$\frac{\partial F_i}{\partial t}+\frac{\partial (F_i u)}{\partial x}+\frac{\partial (F_i v)}{\partial y}+\frac{\partial (F_i w)}{\partial z}=0 \tag{3a}$$

$$\sum_{i=1}^{2} F_i = 1 \tag{3b}$$

where, F_i represents the volume fraction of the ith phase. In this paper, a finite volume method (FVM)-based CFD software, ANSYS Fluent, is used to establish the NWT. A pushing-board method is applied to generate expected regular liner waves in the left boundary of NWT, and following equations can describe the motion of pushing-board:

$$x_b(t)=\frac{S_0}{2}\sin \omega t \tag{4a}$$

$$u_b(t) = \frac{\omega S_0}{2}\cos\omega t \tag{4b}$$

where, t is the flow time; $x_b(t)$ and $u_b(t)$ represent the displacement and velocity of pushing-board respectively; ω is the wave frequency; S_0 is the stroke of pushing-board, which is related to the parameters of the expected wave. The surface elevation of wave generated by pushing-board can be expressed as Equation (5a), from which the relationship between S_0 and the parameters of the expected wave can be obtained as Equation (5b):

$$\eta(x,t) = \frac{S_0}{2}\frac{4\sinh^2(kd)}{2kd+\sinh(2kd)}\cos(kx-\omega t) = \frac{H}{2}\cos(kx-\omega t) \tag{5a}$$

$$S_0 = \frac{2kd+\sinh(2kd)}{4\sinh^2(kd)}H \tag{5b}$$

where, η is the wave surface elevation; k represents the wave number; d represents the water depth; H represents the wave height. The velocity of the pushing-board is controlled as Equation (4b) by Users Define Function (UDF) of Fluent, and then the wave in Equation (5a) can be generated. A wave absorbing region is set at the end of the tank to eliminate the reflection wave, where the linearly increasing damping is applied, and the damping source terms are added into the momentum equations. Therefore, the Navier-Stokes equations in damping wave absorbing region can be written as:

$$\frac{\partial u}{\partial t}+u\frac{\partial u}{\partial x}+v\frac{\partial u}{\partial y}+w\frac{\partial u}{\partial z} = -\frac{1}{\rho}\frac{\partial p}{\partial x}+\nu(\frac{\partial^2 u}{\partial x^2}+\frac{\partial^2 u}{\partial y^2}+\frac{\partial^2 u}{\partial z^2})-\mu(x)u \tag{6a}$$

$$\frac{\partial v}{\partial t}+u\frac{\partial v}{\partial x}+v\frac{\partial v}{\partial y}+w\frac{\partial v}{\partial z} = -\frac{1}{\rho}\frac{\partial p}{\partial y}+\nu(\frac{\partial^2 v}{\partial x^2}+\frac{\partial^2 v}{\partial y^2}+\frac{\partial^2 v}{\partial z^2})-\mu(x)v \tag{6b}$$

$$\frac{\partial w}{\partial t}+u\frac{\partial w}{\partial x}+v\frac{\partial w}{\partial y}+w\frac{\partial w}{\partial z} = -\frac{1}{\rho}\frac{\partial p}{\partial z}+\nu(\frac{\partial^2 w}{\partial x^2}+\frac{\partial^2 w}{\partial y^2}+\frac{\partial^2 w}{\partial z^2})-g-\mu(x)w \tag{6c}$$

where, the damping coefficient $\mu(x)$ is expressed as:

$$\mu(x) = \alpha\frac{(x-x_1)}{(x_2-x_1)} \tag{7}$$

where, x_1 and x_2 are the start and end of wave absorbing region; α is an empirical coefficient, usually taken as 3.0~12.0 s^{-1} and is set as 8.0 s^{-1} in this paper after comparing the wave elimination effect.

The bottom and the side boundaries of the NWT are set as full-slip walls, and the top boundary is set with pressure out condition.

3.2 Pressure drop of porous cylinder

The volume-averaged macro-scale model to represent the impact of the porous structure on the flow can traced back to Darcy's work for water flowing through sand (Darcy, 1856), where the hydraulic gradient is assumed to be linearly proportional to the flow passing through, as shown in the following equation:

$$I = -\frac{1}{\rho g}\frac{\partial p}{\partial x} = a_p \bar{u} \tag{8}$$

where, I is the hydraulic gradient, a_p is an empirical coefficient. $\bar{u}$ is averaged discharge velocity. Forcheimer (1901) extended Darcy's law by adding a quadratic term, thus more energetic flows under high Reynolds number can be considered:

$$I = -\frac{1}{\rho g}\frac{\partial p}{\partial x} = a_p \bar{u} + b_p \bar{u}\left|\bar{u}\right| \tag{9}$$

where, b_p is an empirical coefficient. Polubarinova-Kochina (1962) further considered the added mass effects of unsteady flows and added a transient term:

$$I = -\frac{1}{\rho g}\frac{\partial p}{\partial x} = a_p \bar{u} + b_p \bar{u}\left|\bar{u}\right| + c_p \frac{\partial \bar{u}}{\partial t} \tag{10}$$

where, c_p is an empirical coefficient. For thin porous barrier, the pressure drop ΔP of water flow passing through can be expressed as (Sollitt and Cross, 1972):

$$\frac{\Delta P}{\rho} = \frac{\nu U_n}{l} + \frac{C_f}{2} U_n \left|U_n\right| + c\frac{\partial U_n}{\partial t} \tag{11}$$

where, U_n represents the velocity normal to the porous surface, l is a length scale, which is related to geometry characteristics of porous structures; c is an inertial coefficient; C_f is a dimensionless friction coefficient, which can be expressed as (Molin, 2011):

$$C_f = \frac{1-\varepsilon}{\varepsilon^2 \delta} \tag{12}$$

where, δ is the discharge coefficient, which is usually set as 0.4-0.5 (Liu and Li, 2017) and is set as 0.5 in this paper. The first term in the right of Equation (11) is a linear viscous friction term, the second term is a quadratic turbulent dissipation term, and the third term is a transient inertia term. The linear viscous friction term is dominant at low Reynolds number while the quadratic turbulent dissipation term becomes dominant at high Reynolds number (Sollitt and Cross, 1972). The Reynolds numbers for wave interaction with thin porous plates are usually sufficiently high so that the linear viscous friction term can be neglected (Mackay and Johanning, 2020). The transient inertia term accounts for added mass effects and transient interaction between the fluid and porous structures, where the inertial coefficient is related to the geometries of porous structures. In this paper, the empirical equation to calculate the inertial coefficient proposed by McIver (1998) for porous barrier of circular holes is adopted:

$$\frac{c}{s} \approx 0.3898\varepsilon - 0.03239\sqrt{\varepsilon} + 1.2415 + \frac{0.8862}{\sqrt{\varepsilon}} \tag{13}$$

where, s represents the distance between adjacent hole centers.

To model the wave flow passing through the porous surface in the NWT, the pressure drop per unit thickness need to be added into momentum equations in the geometric region of porous media as source terms, which can be assumed to be of either isotropic or anisotropic nature. The study of Feichtner et al. (2021) illustrates that there is nearly no difference between isotropic and anisotropic pressure drop for modeling wave-porous structures interaction. In contrast to similar work by Feichtner et al. (2020), this work uses an orthotropic (as a sub-category of anisotropic) implementation to represent the porous barrier. This means that the pressure drop only occurs in the direction perpendicular to the porous surface. According to Equation (11) the magnitude of added source term S_{porous} can be expressed as:

$$S_{porous} = -\frac{1}{\rho}\frac{\Delta P}{\Delta n} = -\frac{1}{\Delta n}\left(\frac{C_f}{2}U_{\mathrm{n}}\left|U_n\right| + c\frac{\partial U_n}{\partial t}\right) \tag{14}$$

where, Δn is the thickness of porous cylinder region. In the cylindrical coordinates system, the added source terms in three directions can be expressed as:

$$S_x = S_{porous}\cos\theta \tag{15a}$$

$$S_y = S_{porous}\sin\theta \tag{15b}$$

$$S_z = 0 \tag{15c}$$

where, S_x , S_y and S_z are the source term in three directions respectively; θ is the angle between the radial direction of the cylinder and the positive direction of x axis, which is converted in the CFD code according to the relative relationship between the Cartesian coordinate system of the NWT and the cylindrical coordinate system of porous cylinder.

4 Single Porous cylinder

4.1 Computational domain setup

Figure 8 shows the sketch of NWT for wave interaction with single porous cylinder shell. The NWT is set as 25m long, including a 10m-long wave absorbing region, and the width and height are 3m and 1.5m, respectively. The bottom and the side boundaries of the NWT are set as full-slip walls, and the top boundary is set with pressure out condition, which ensures that the boundaries in CFD model is consistent with the tank tests. The center of porous cylinder is set as 10m away from the wave generation boundary. The porous cylinder is fixed and vertical relative to the direction of the waves. Seven numerical wave probes are set to monitor the wave heights, where WP1-WP5 are set the same as the experiments, WP6 is set to monitor the reflected wave at the end of the NWT, and WPO is set in the center of porous cylinder to monitor the wave elevation here.

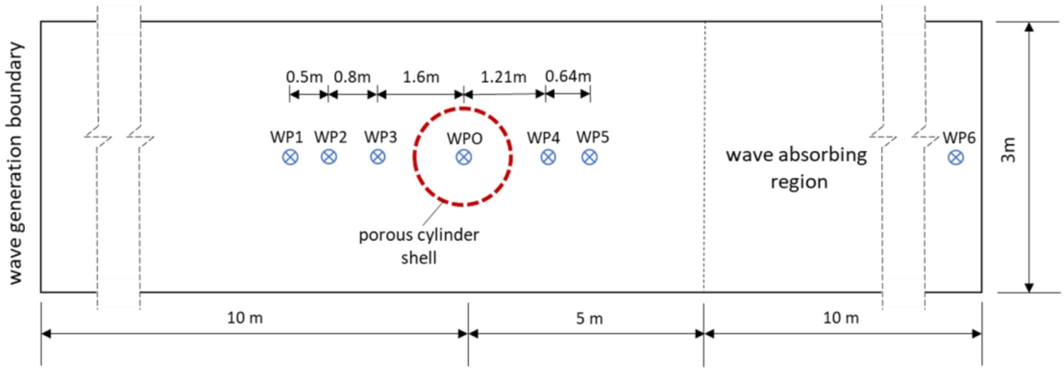

Figure 8 Sketch of NWT for wave interaction with single porous cylinder shell (plan view)

As shown in Figure 9, the mesh was generated as a block-structured hexahedral mesh, the sizes of mesh cells are set as follows: in X-direction, the cell size in the wave generation region is refined as 1/10 of S_0, in the wave propagation region is refined as 1/*M* of wavelength, and in the wave absorbing region is gradually growing with a start ratio of 1.20; in Z-direction, the cell size of one wave height above and below the water surface is defined to 1/*N* of the wave height, and changes to sparse gradually in the remaining region with a start ratio of 1.05; the cell size in porous cylinder region is defined as 1/*R* of the cylinder thickness, and changes to sparse gradually in the remaining region with a start ratio of 1.05.

The mesh size parameters *M*, *N*, and *R* are determined by the mesh convergence study. Firstly, the mesh convergence study for free surface elevations has been carried out by a 2D empty NWT. Table 1 shows a summary of the mesh convergence study for the free surface region looking at the surface elevation at WP1 in terms of different *M* and *N*, where the same wave condition (*T*=1.9s, *H*=0.0772m, *d*=1.0m, *L*=4.85m) is applied. After comparing the wave surface elevations under four different mesh types with the input values, the mesh type II with *M*=160, *N*=10 is selected due to its sufficient simulation precision and a relatively low number of mesh cells.

Secondly, the mesh convergence study for horizontal wave force on the porous cylinder has been carried out by a 3D NWT and a porous cylinder with porosity *ε*=0.2 and radius $a_1 = 0.25\text{m}$. Table 2 shows a summary of the mesh convergence study for the averaged wave force amplitude, where, the same wave condition (*T*=1.9s, *H*=0.0772m, *d*=1.0m, *L*=4.85m) is applied and *M*=160, *N*=10 is fixed. After comparing the wave surface elevations under four different mesh types with the input values, the mesh type VI with *R*=10 is selected due to its sufficient simulation precision and a relatively low number of mesh cells.

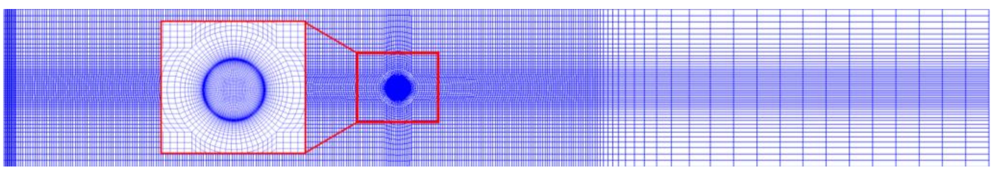

(a) Plan view

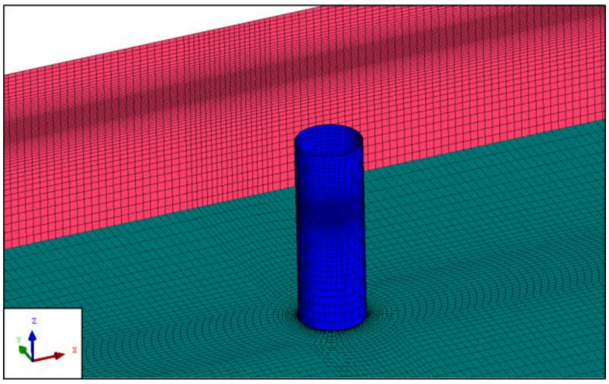

(b) Perspective view

Figure 9 Generated mesh for NWT and a single porous cylinder shell

Table 1 Simulation results of wave height under different mesh types

Mesh type	M	N	Δx (mm)	Δy(mm)	H(m)	Error
I	80	5	60.6	15.4	0.0763	-1.15%
II	160	10	30.3	7.7	0.0768	-0.52%
III	240	15	20.2	5.1	0.0768	-0.52%
IV	320	20	15.2	3.9	0.0769	-0.39%

Table 2 Simulation results of wave force under different mesh types

Mesh type	M	N	R	Δr (mm)	F (N)	Error
V	160	10	5	1.0	32.56	-
VI	160	10	10	0.5	33.82	3.87%
VII	160	10	15	0.33	34.25	1.30%
VIII	160	10	20	0.25	34.37	0.32%

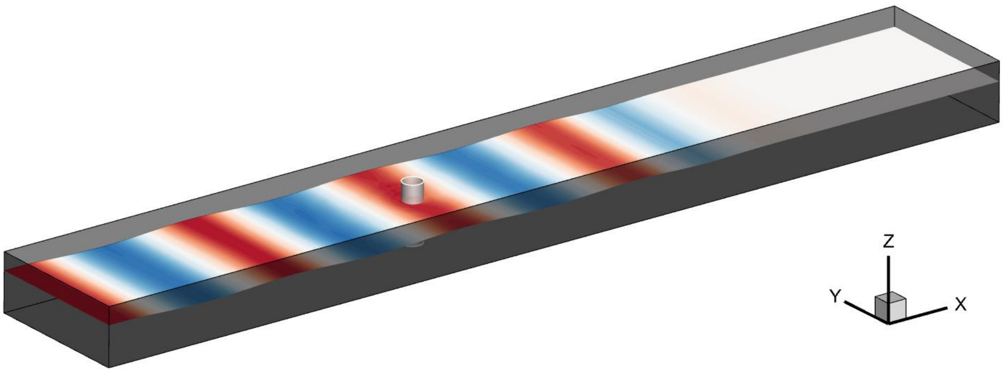

Figure10 Snapshot of the 3D numerical model of wave interaction with a porous cylinder

In this section, a series of porous cylinder with porosities of 0.1, 0.2, 0.3 and diameters of 0.375m, 0.50m, 0.75m are simulated with fixed thickness of 1cm and height of 1.5m. Partly wave conditions conducted in tank tests are adopted, and the snapshot of the 3D numerical model is shown in Figure 10.

4.2 *Free-surface elevation*

Figure 11 shows the comparison of time series of free surface elevation for CFD and experimental results with the porosity ε=0.2 and radius $a_1 = 0.25\text{m}$. Due to space limitation, comparisons are presented only one wave condition, and the results of other wave conditions are summarized in Table 3 in the form of average wave heights. It can be seen that the CFD model can well replicate the free surface elevation monitored by WP1-WP5 in experiments, and the maximum difference of wave heights are within 10%.

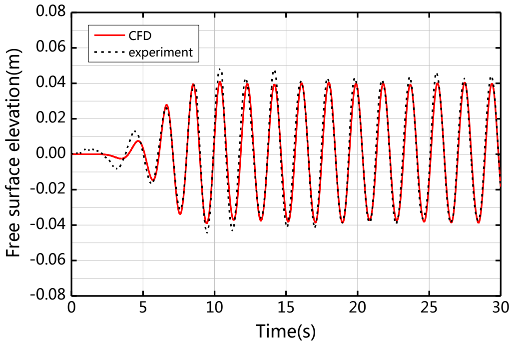

(a) WP1

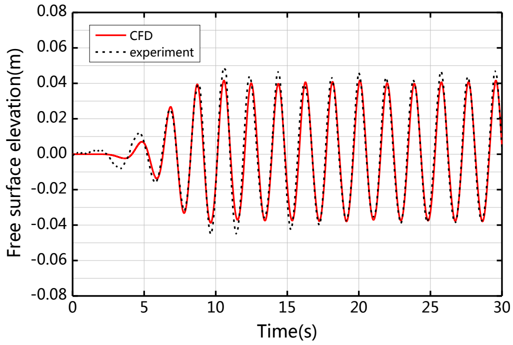

(b) WP2

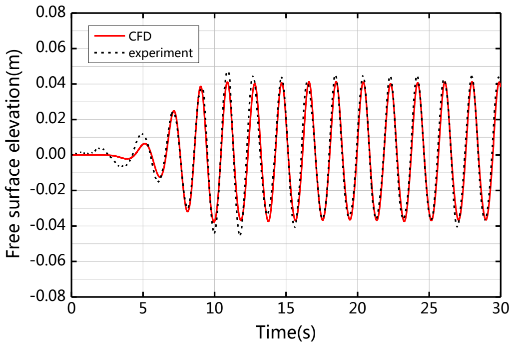

(c) WP3

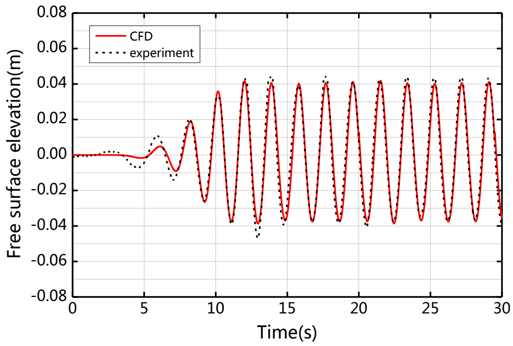

(d) WP4

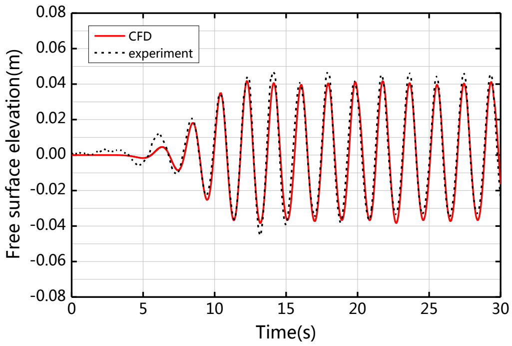

(e) WP5

Figure 11 Time series of free surface elevation of WP1~WP5 (T=1.9s, H=0.0772m, d=1.0m)

Table 3 Comparison of wave heights monitored by WP1~WP5 under different wave conditions (m)

Wave conditions	H=0.0300m, T=1.1s			H=0.0533m, T=1.5s			H=0.0772m, T=1.9s		
Wave probes	Exp.	CFD	Relative difference	Exp.	CFD	Relative difference	Exp.	CFD	Relative difference
WP1	0.0331	0.0299	-9.67%	0.0541	0.0524	3.14%	0.0837	0.0786	6.09%
WP2	0.0320	0.0304	-5.00%	0.0523	0.0542	-3.63%	0.0803	0.0761	5.23%
WP3	0.0304	0.0314	3.29%	0.0562	0.0559	0.53%	0.0841	0.0758	9.87%
WP4	0.0295	0.0312	5.76%	0.0524	0.0557	-6.30%	0.0858	0.079	7.93%
WP5	0.0286	0.0304	6.29%	0.0535	0.0541	-1.12%	0.0796	0.0762	4.27%
Wave conditions	H=0.1001m, T=2.3s			H=0.1221m, T=2.7s			H=0.1437m, T=3.1s		
Wave probes	Exp.	CFD	Relative difference	Exp.	CFD	Relative difference	Exp.	CFD	Relative difference
WP1	0.1060	0.0981	-7.45%	0.1318	0.12	8.95%	0.1329	0.1411	-6.17%
WP2	0.1068	0.1014	-5.06%	0.1314	0.124	5.63%	0.1303	0.1408	-8.06%
WP3	0.1036	0.1046	0.97%	0.1325	0.1279	3.47%	0.1422	0.1504	-5.77%
WP4	0.1055	0.1041	-1.33%	0.1354	0.1274	5.91%	0.1411	0.1498	-6.17%
WP5	0.0988	0.1012	2.43%	0.1369	0.1238	9.57%	0.1384	0.1456	-5.20%

Figure 12 shows the water volume fraction and velocity magnitude vectors at the y=2 plane when the wave peak impacting on the porous cylinder. It can be observed that when the incident wave passing through the surface of porous cylinder, obvious wave drop occurs due to the resistance of porous surface. It can be observed from the velocity vectors diagram the variation of velocity at the intersection of porous surfaces and free water surface is very severe, especially the front surface. There is an obvious vortex behind the front surface of the porous cylinder. Figure 13 shows the distribution of velocity magnitudes at the free water surface in and around the porous cylinder when the wave peak impacting on the porous cylinder. It can be observed that the velocity of water flow at the front of porous cylinder decreases due to the resistance of porous surface and further reducing after passing into the porous cylinder. The flow velocity changes to large values at the left and right sides of porous cylinder, reaching at about 0.25m/s, as a contrast, the horizontal velocity of the peak of the incident wave surface is 0.15m/s.

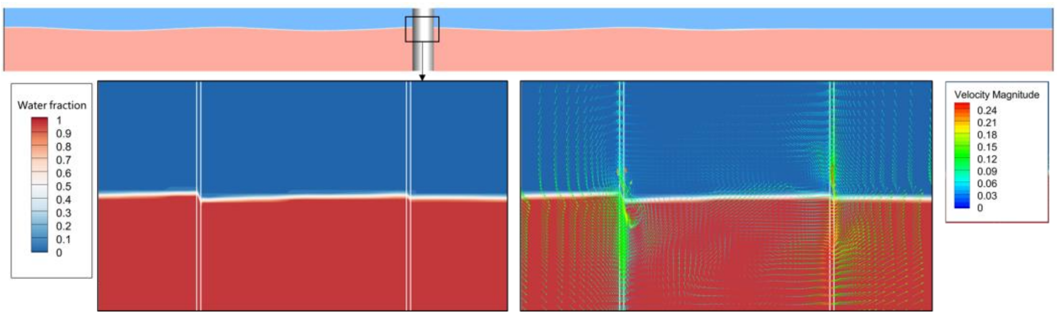

Figure 12 Water volume fraction (left lower) and velocity magnitude vectors (right lower) at the y=2 plane

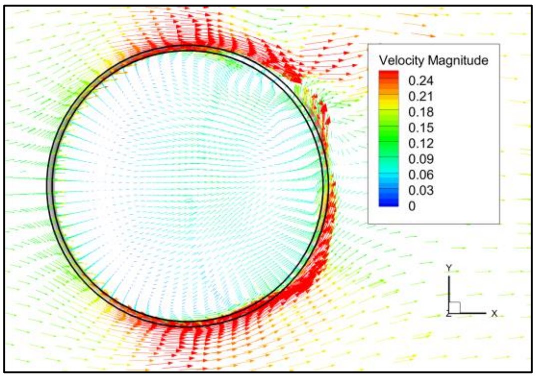

Figure13 Distribution of velocity magnitudes at the free water surface in and around the porous cylinder

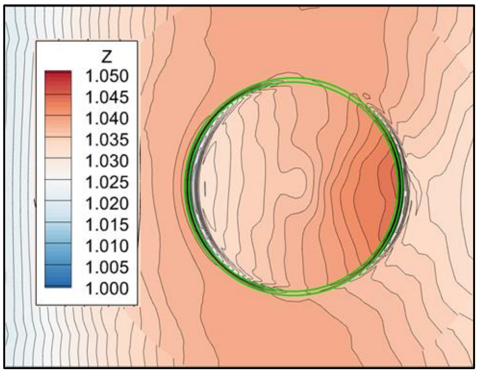

(a) ε=0.3 $a_1/a_0=2.0$

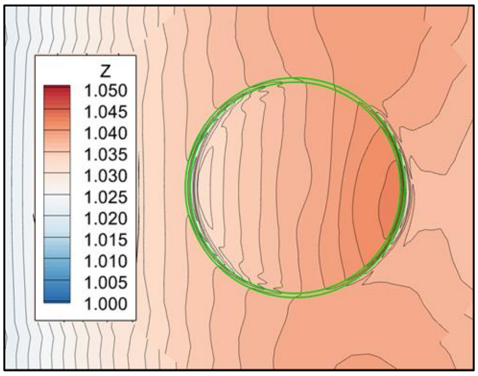

(b) ε=0.2 $a_1/a_0=2.0$

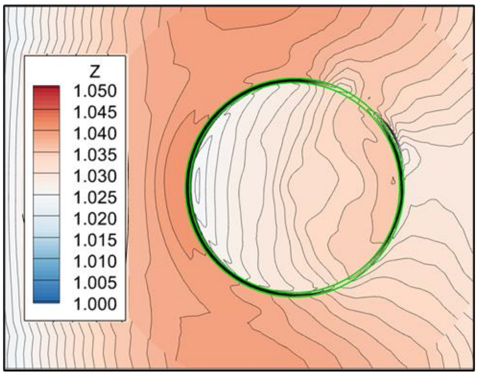

(c) ε=0.1 $a_1/a_0=2.0$

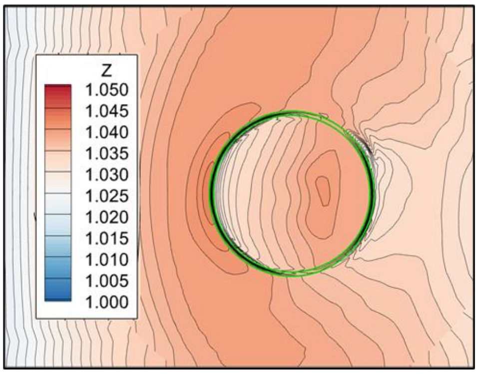

(d) ε=0.2 $a_1/a_0=1.5$

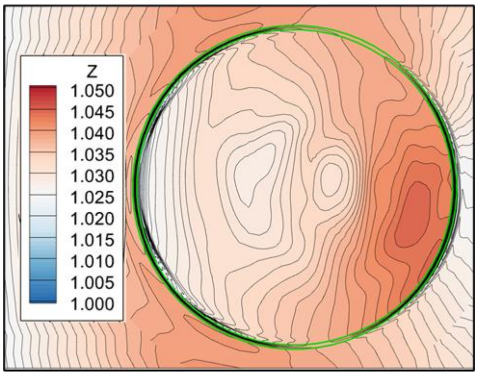

(e) ε=0.2 $a_1/a_0=3.0$

Figure 14 Contours free surface elevations inside the porous cylinders for different porosities and radii under the impact of wave peak from CFD simulations.

Figure 14 shows the contours free surface elevations inside the porous cylinders with different porosities and radii from the CFD simulations. According to Figure 14, when the wave peak impacts on porous cylinder, the internal wave surface is characterized by low front and high rear. On the one hand, the reflection and dissipation effect of front-part cylinder surface makes the wave surface elevation decreased significantly in the front half area; on the other hand, the reflection effect of the rear-part cylinder surface makes the wave surface elevation rising significantly in the rear half area. In order to further quantitatively analyze the influence of different porosity and radius on the wave surface inside the porous cylinder, the wave height at the center point of the cylinder monitored by WPO and calculated, as shown in Figure 15. H_i is the incident wave heights, H_m represents the monitored wave heights by WPO, which are similarly obtained from the periodically steady signal section of time series results and calculated by standard-deviation (*STD*) as follow:

$$H_m = 2\sqrt{2}STD(\eta(t)) \tag{16}$$

where, $\eta(t)$ is the time series of wave surface elevation and data of last five stable periods from CFD and the corresponding period of the experiment are used in the calculation of the *STD*.

According to Figure 15(a), a larger porosity leads to a larger wave height inside the porous cylinder. It is obvious that a larger porosity leads to more wave transmitting through the front surface of porous cylinder, thus causing a larger wave elevation inside. According to Figure 15(b), the effect of diameter on the wave heights inside porous cylinder is not monotonous as that of porosity, and the smallest wave height appears when $a_1/a_0 = 2.0$. For the porous cylinders of ε=0.2, $a_1/a_0 = 1.5$, the inside wave heights are larger than incident wave for several wave conditions. The reason is that while the porous cylinder can reduce the transmitted wave by dissipating wave energy, its cylindrical surface can also focus wave to the center. Under certain wave frequency and cylinder diameter, the focusing reflection leads to the inside wave heights larger than incident wave.

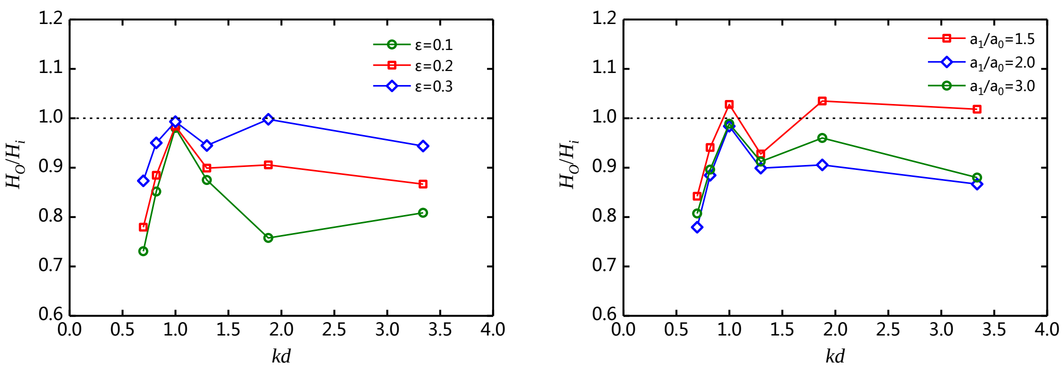

(a) (b)

Figure15 Relative wave heights inside porous cylinder against *kd* from CFD method: (a) For porous cylinder of various porosities; (b) For porous cylinders with various radii

4.3 *Wave force on porous cylinder*

Figure 16 shows the comparison of time series of horizontal wave force for CFD and experimental results. For the convenience of comparing the results of CFD method and experiment, the phase position of experimental results is adjusted to be consistent with CFD results. According to Figure 16, the CFD results are nearly identical with experimental ones in period, and in terms of wave force amplitude, although some differences can be observed, the CFD results are also consistent with experimental ones in general. It is also observed that the shoreward wave force is larger than the seaward wave force, which is due to the higher crests and lower troughs of the incident wave. Figure 17 summarizes the average shoreward wave force against the seaward wave force from Figure 16, and it is found that the larger period and wave height, the bigger difference between the shoreward force and seaward force. The mean horizontal wave force amplitudes are obtained from the periodically steady signal section of time series results and are calculated by standard-deviation (*STD*) as follow:

$$F_x = \sqrt{2}STD(F(t)) \tag{17}$$

where, F_x represents the horizontal wave force amplitude; $F(t)$ is the time series of horizontal wave force and data of last five stable periods from CFD and the corresponding period of the experiment are used in the calculation of the *STD*.

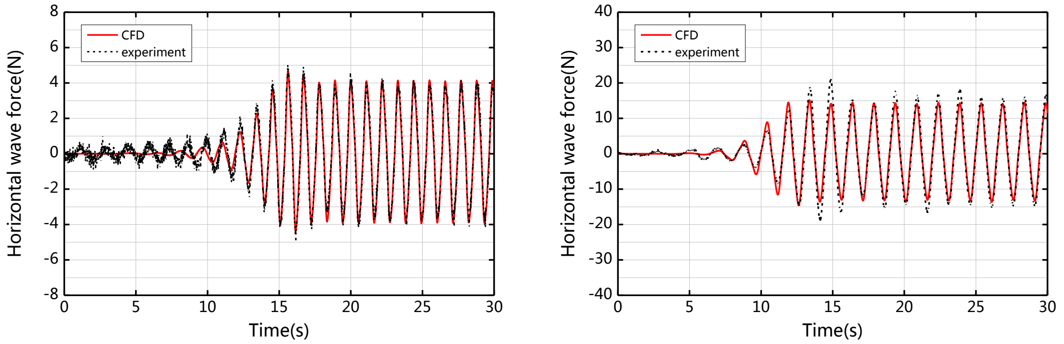

(a) T=1.1s, H=0.0300m (b) T=1.5s, H=0.0530m

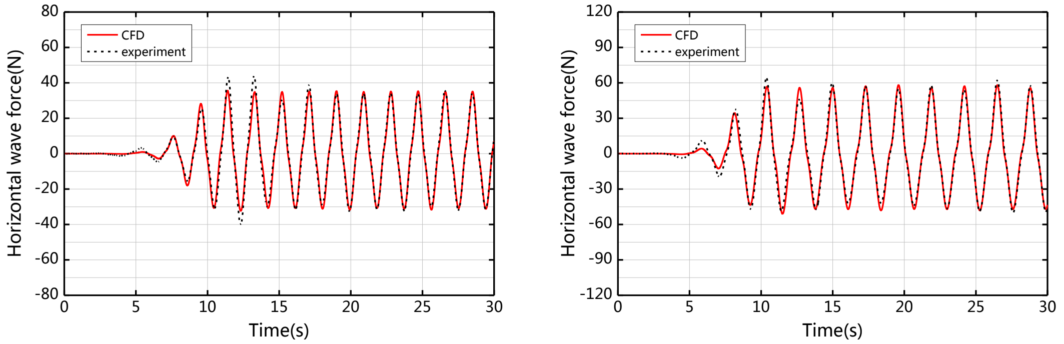

(c) T=1.9s, H=0.0772m (d) T=2.3s, H=0.1001m

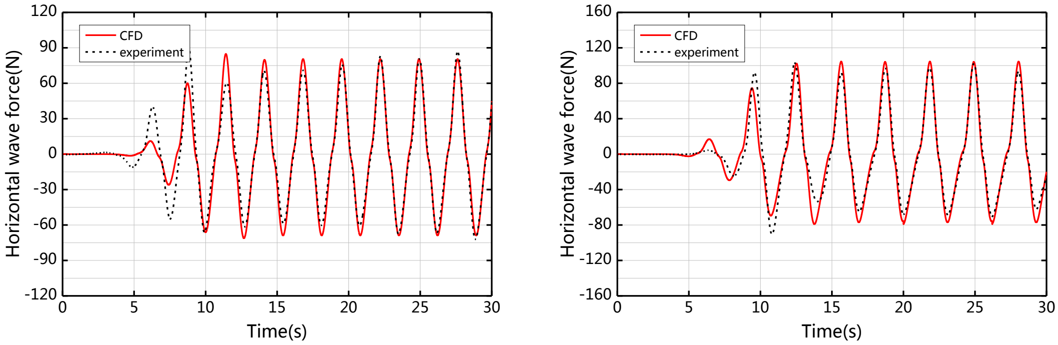

(e) T=2.7s, H=0.1221m (f) T=3.1s, H=0.1437m

Figure 16 Time series of horizontal wave force on porous cylinder

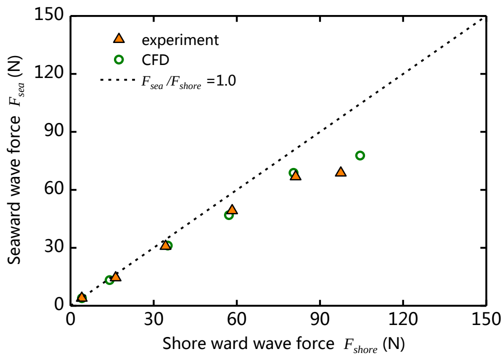

Figure 17 Seaward wave force against shoreward wave force on porous cylinder

For further evaluating the reliability of the present CFD method, the wave force amplitude is analyzed by comparing the CFD results, the experimental results, the results of Mackay et al. (2020) by a BEM model with a quadratic pressure-drop condition, and the results calculated by a linear potential flow model from Cong and Liu (2020). The 'porous-effect parameter' in the linear potential flow model is set constant and assumed appropriate for deep water. Figure 18 shows the normalized wave force amplitudes on porous cylinder obtained from the four approaches above with a constant wave slope kA=0.050, where the normalized wave force amplitudes are defined as:

$$f_x = F_x / \rho g A d^2 \tag{18}$$

where, f_x is the normalized value; d is the water depth.

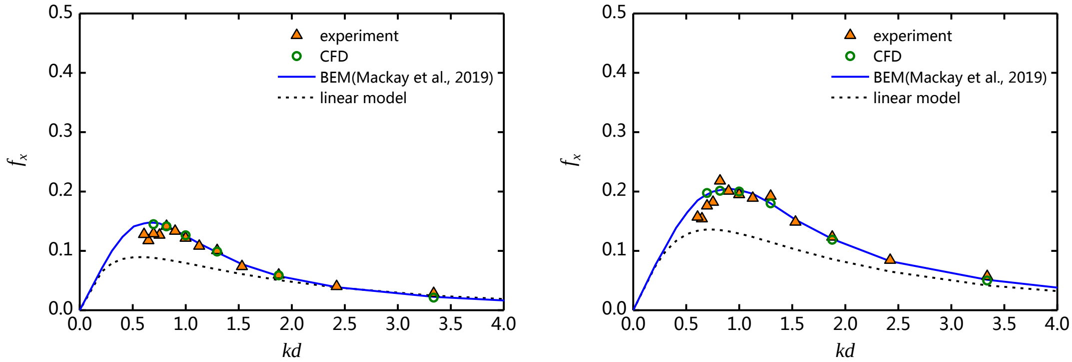

(a) ε=0.3, $a_1/a_0 = 2.0$ (b) ε=0.2, $a_1/a_0 = 2.0$

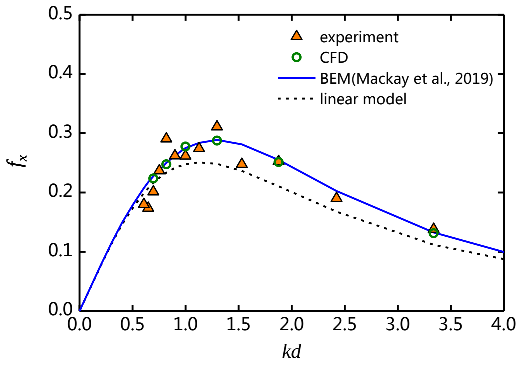

(c) ε=0.1, $a_1/a_0=2.0$

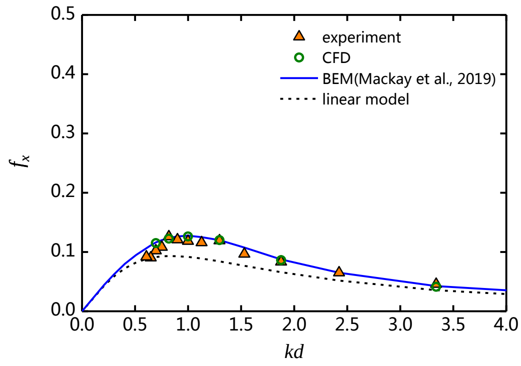

(d) ε=0.2, $a_1/a_0=1.5$

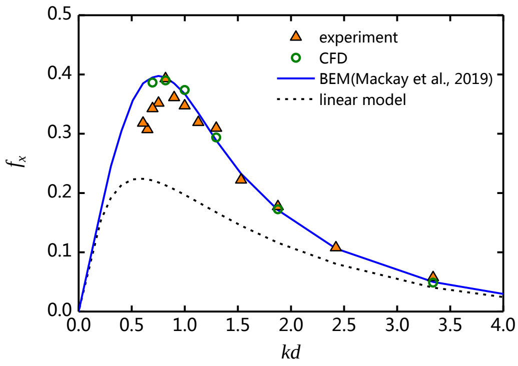

(e) ε=0.2, $a_1/a_0=3.0$

Figure 18 Normalized wave force on porous cylinder against *kd* with different geometrical parameters (kA =0.050, a_0 =0.125m)

According to Figure 18, under the assumption of 'porous-effect parameter' appropriate for deep water, the wave forces replicated by the linear model obviously underestimates compared with experimental results in this paper, especially when the normalized wave force reaching peak values at low frequencies. By contrast, the CFD method and BEM model can well replicated the wave forces monitored by experiments, due to both of which adopted the more accurate quadratic pressure-drop condition. Furthermore, the present CFD method considered viscous force when calculating the wave force on porous cylinder, but in these cases, compared to the dominant pressure force, the viscous force contribution to the wave force is very small and the effects of nonlinearities in the wave-structure interaction are relatively small.

The effects of porosity on the wave force on porous cylinder can be analyzed from Figure 18(a)(b)(c), where the diameter of porous cylinder is fixed as 0.50m, and the porosities are 0.1, 0.2 and 0.3. It can be learned that the larger porosity is, the smaller wave force is. It is obvious that a porous cylinder with a larger porosity lets a larger proportion of the wave pass through the porous surface, meaning that a smaller area of porous surface impacted by waves, thus reducing the wave force. From the perspective of the pressure drop model, a larger porosity leads to a decrease on the quadratic turbulent dissipation term, so that the pressure drop through the porous cylinder surface decreases and thus reduces the wave force. The effects of radius on the wave force on porous cylinder can be analyzed from Figure 18(b)(d)(e), where the porosity of porous cylinder is fixed as 0.2, and the diameters are 0.375m, 0.50m and 0.75m. It can be learned that a larger diameter leads to a larger wave force on cylinder, which is mainly because the porous cylinder frontal surface area increases with the increasing of cylinder diameter, meaning that the wave impacting area increases and thus causing the increase of wave force. It can be confirmed from analysis above that the pressure loss model has well simulated the macroscopic hydrodynamic performance of porous cylinder and present CFD method can well replicate the wave force.

5 Porous cylinder with solid inner column

5.1 Computational domain setup

Figure 19 shows the sketch of NWT for wave interaction with porous cylinder shell with an inner solid column, which is similar with the NWT created in section 4. The only one difference is that there are four wave probes set around the inner solid column (WPA-WPD). Figure 20 shows the generated mesh for these series of simulations.

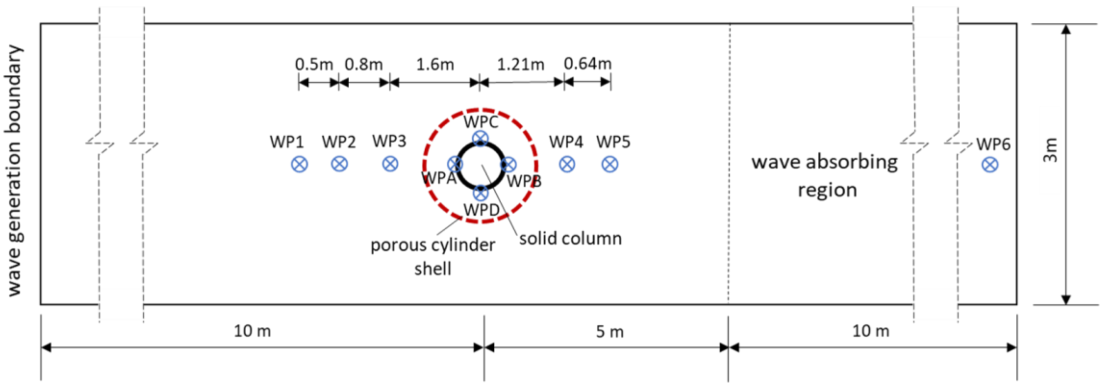

Figure 19 Sketch of NWT for wave interaction with porous cylinder shell with an inner solid column (plan view)

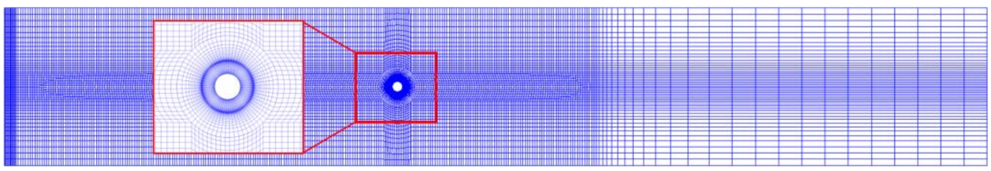

(a) Plan view

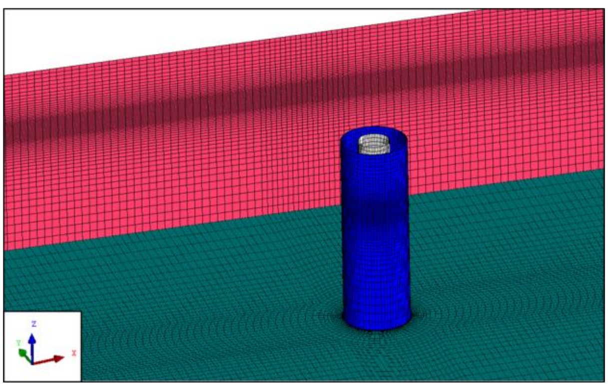

(b) Perspective view

Figure 20 Generated mesh for NWT and porous cylinder shell with an inner solid column

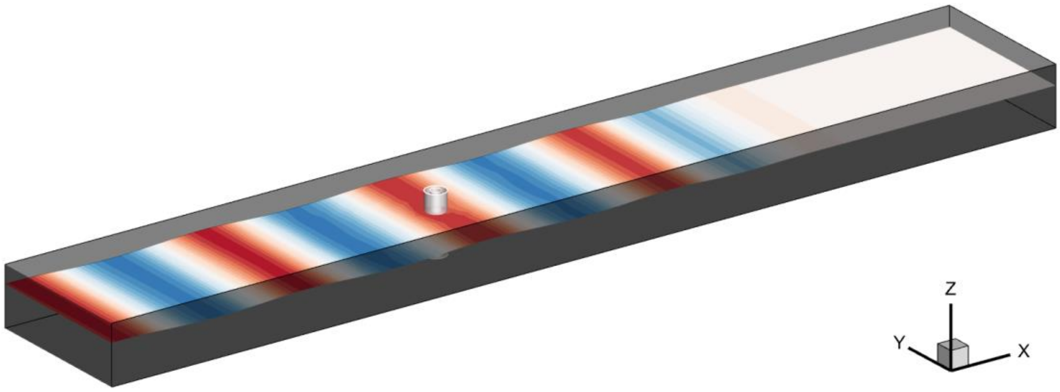

Figure 21 Snapshot of the 3D numerical model of wave interaction with the combine cylindrical structure

In this section, a series of combined cylindrical structures with porosities of 0.1, 0.2, 0.3 and outer diameters of 0.375m, 0.50m, 0.75m are simulated with fixed thickness of 1cm and height of 1.5m. Partly wave conditions conducted in tank tests are adopted, and the snapshot of the 3D numerical model is shown in Figure 21.

5.2 *Free-surface elevation*

A comparison of the time series of free surface elevation for the CFD and experimental results are similar as shown in Section 4.2, and the CFD model can also well replicate the free surface elevation measured by WP1-WP5 in the experiments, and the error differences in wave heights are also within 10%.

Figure 22 shows the water volume fraction and velocity magnitude vectors at the y=2 plane when the wave peak impacting on the combined cylindrical structure. Similar wave drop and vortex caused by porous cylinder surface are observed. Figure 23 shows the distribution of velocity magnitudes at the free water surface in and around combined cylindrical structure when the wave peak impacting on the porous cylinder. It can be observed that the velocity of water flow at the front of porous cylinder and inner cylinder decreases due to the resistance of porous surface and solid wall. The flow velocity changes to large values at the left and right sides of both porous cylinder and inner cylinder, reaching at about 0.25m/s, as a contrast, the horizontal velocity of the peak of the incident wave surface is 0.15m/s.

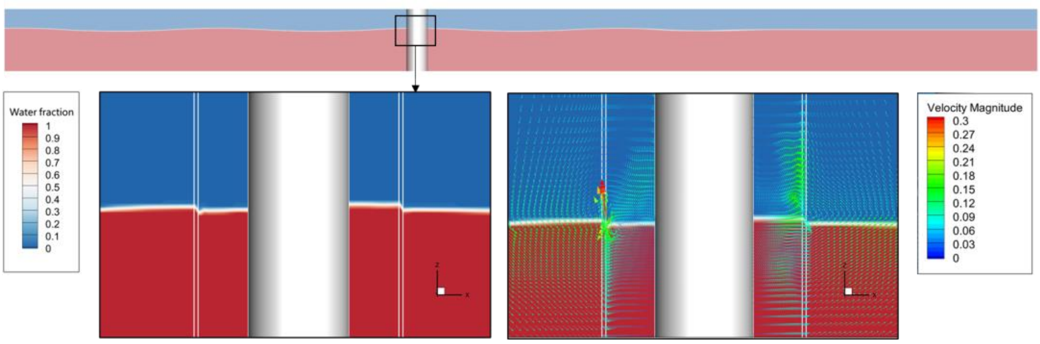

Figure 22 Water volume fraction (left lower) and velocity magnitude vectors (right lower) at the y=2 plane

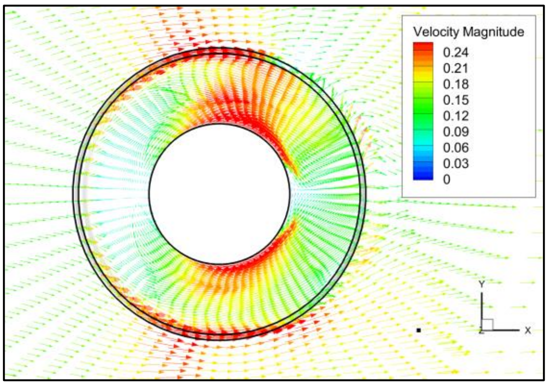

Figure 23 Distribution of velocity magnitudes at the free water surface in and around the porous cylinder and inner solid column

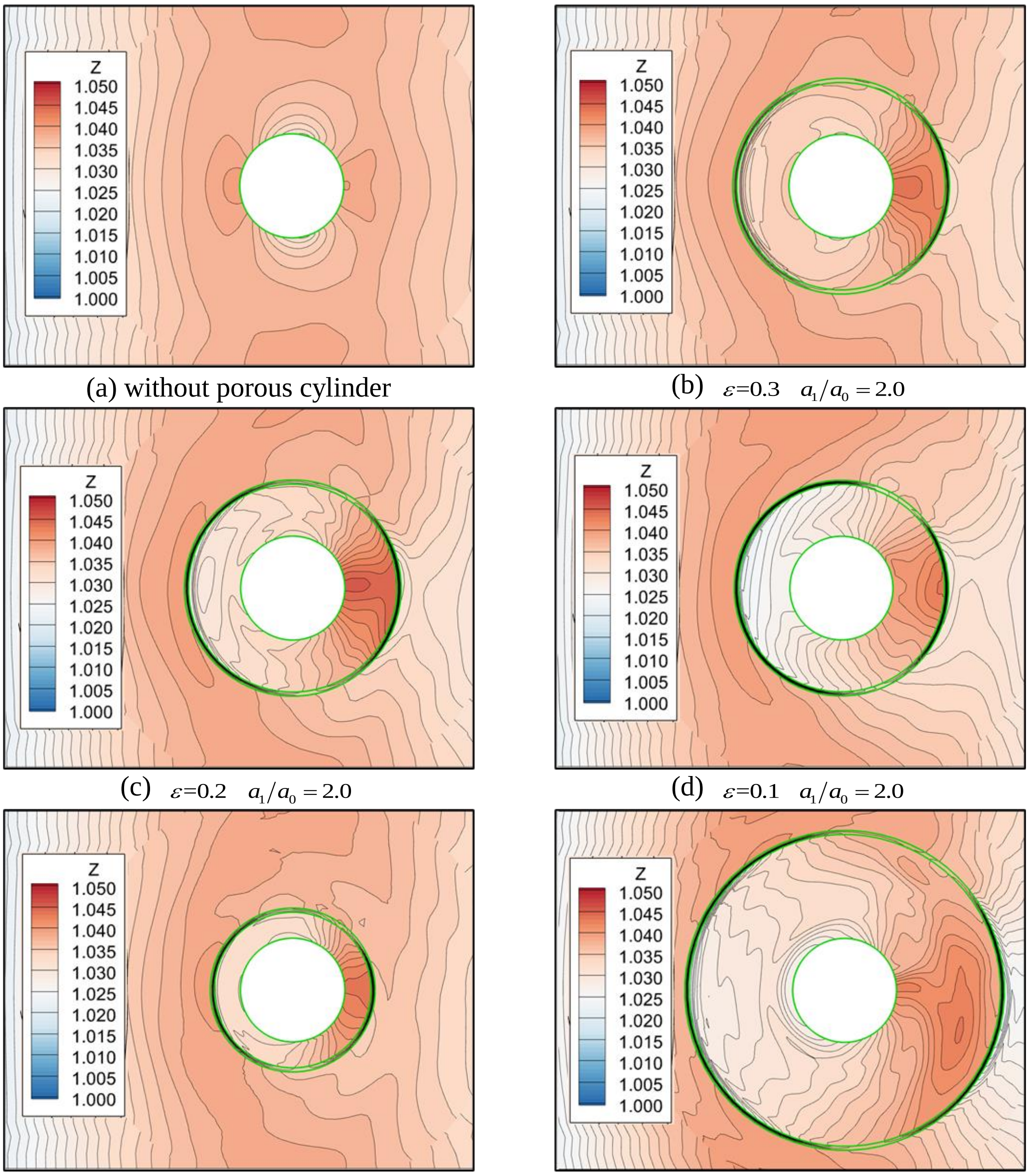

(a) without porous cylinder (b) ε=0.3 $a_1/a_0 = 2.0$

(c) ε=0.2 $a_1/a_0 = 2.0$ (d) ε=0.1 $a_1/a_0 = 2.0$

(e) ε=0.2 $a_1/a_0 = 1.5$ (f) ε=0.2 $a_1/a_0 = 3.0$

Figure 24 Contours of wave surface elevation for different porosities and radii from CFD simulations: (a) for a single solid column under the impact of wave peak; (b)~(f) for a porous cylinder with a solid inner column under the impact of wave peak

Figure 24 shows the contours free surface elevations inside the combined cylindrical structures with different porosities and radii from the CFD simulations. According to Figure 24(a), the wave surface at front of the solid cylinder is obviously higher than incident wave, the wave surface at the rear of cylinder is slightly increased, and the wave surface at left and right sides are slightly decreased. After adding a porous cylinder, when the wave peak impacting, the internal wave surface is characterized by low front and high rear. On the one hand, the reflection and dissipation effect of front-part cylinder surface makes the wave surface elevation decreased significantly in the front half area; on the other hand, the reflection effect of the rear-part cylinder surface makes the wave surface elevation rising significantly in the rear half area. In order to further quantitatively analyze the influence of different porosity and radius on the wave surface inside the combined cylindrical structures, the wave height monitored by WPA~WPC (the waves monitored by WPD is nearly same with those by WPC) and calculated, as shown in Figure 25. According to Figure 25(a)(b)(e)(f), for WPA and WPC, all the monitored wave heights with a porous cylinder are smaller than those without. Especially for WPA, the reduction of wave heights is obvious, meaning that the wave elevation at the front of solid column are effectively reduced by the added porous cylinder. The porosity and outer radius have effects on the reduction of wave heights at WPA and WPC. The larger porosity, the larger wave heights at WPA and WPC, which is mainly because the large porosity increases the transmitted wave. The effect of outer radius on wave heights reduction at WPA and WPC has no obvious monotonous pattern like that of porosity. The explanation is that the variation of outer radius influences the phases of multiple focusing reflection waves on the interlayer, causing the monitored wave heights to be reduced in different degrees for various wave conditions (wave lengths). According to Figure 25(c)(d), for WPB, the wave heights with a porous cylinder are not obviously reduced, even increased under some conditions, which means that a porous cylinder has no ideal wave reduction effectiveness on the back side of solid column. This is because significant wave reflection occurs at the back side of the porous cylinder, causing wave heights at WPB to be increased. On the whole, when an outer radius of $a_1/a_0 = 2.0$ or $a_1/a_0 = 3.0$, the wave heights at the front and side of the solid column are obviously reduced and wave heights at the backside of solid column stays approximately the same.

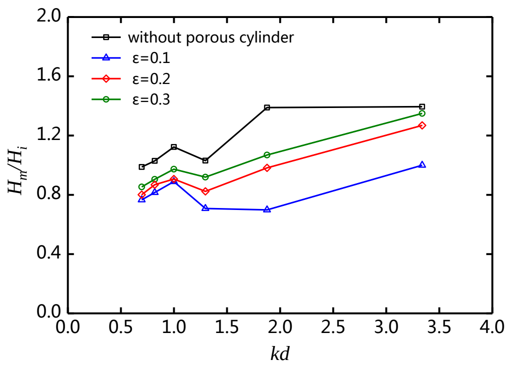

(a) WPA for various porosities

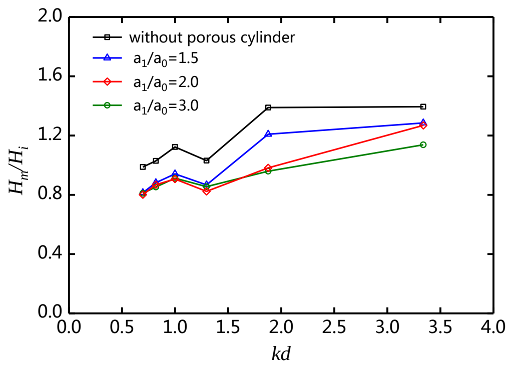

(b) WPA for various outer radii

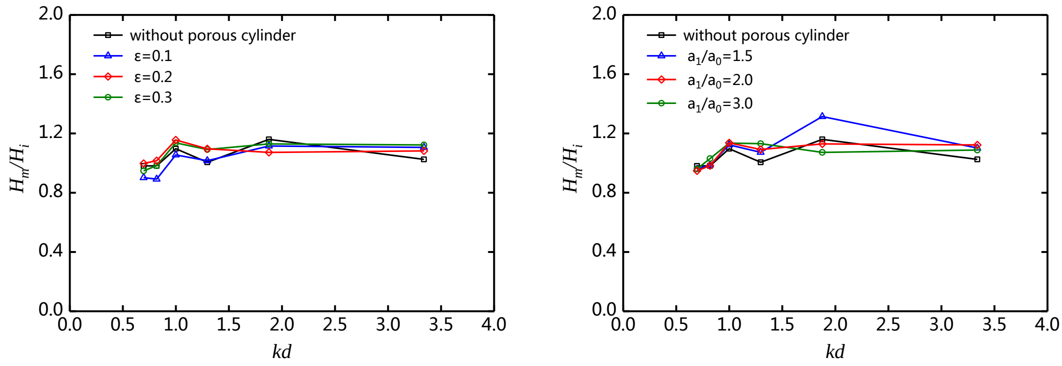

(c) WPB for various porosities (d) WPB for various outer radii

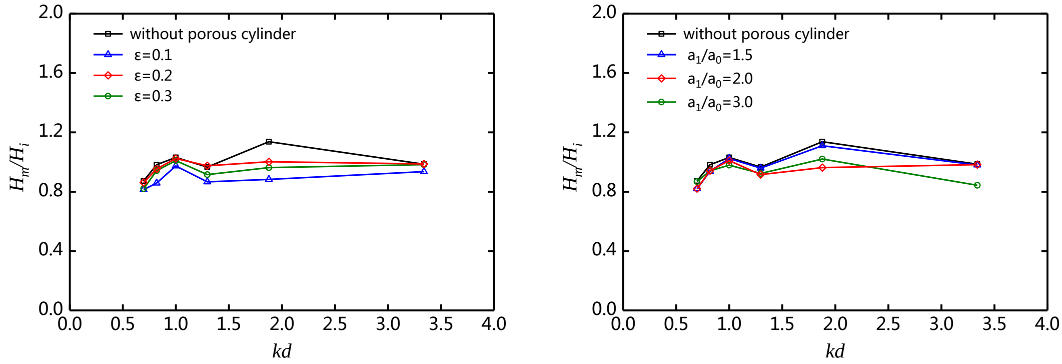

(e) WPC for various porosities (f) WPC for various outer radii

Figure 25 Relative wave heights between porous cylinder and solid column against *kd* from CFD method

5.3 Wave force on the combined structure

Figure 26 shows the comparison of the time sires of horizontal wave force for combined cylindrical structure between the CFD and experimental results, in which the total wave force is calculated by adding the time series results of the two synchronized force sensors monitoring at the inner and outer cylinders directly. The CFD results are nearly identical with experimental ones in period, and in terms of wave force amplitude, although some differences can be observed, the CFD results are also consistent with experimental ones in general. Similarly, the average shore ward wave force against the seaward wave force from Figure 26 are summarized in Figure 27, and the mean horizontal wave force amplitude is also normalized by Equation (18).

Figure 28 shows the comparison of horizontal wave force amplitude from present CFD methods and experiments, and the linear and quadratic methods used in Section 4. According to Figure 28(a), all the three models match the experimental results well for the cases of no porous cylinder shell. However, for the cases of adding porous cylinder, some differences can be observed. Under the assumption of 'porous-effect parameter' appropriate for deep water, the wave forces replicated by the linear model obviously underestimates compared with experimental results in this paper, especially when the normalized wave force reaching peak values at low frequencies. By contrast, the CFD method and BEM model can well replicated the wave forces, especially for the low wave frequencies, since both models adopted the more accurate quadratic pressure-drop condition. Furthermore, the CFD results are nearly coincident with the results of BEM model, and the reason is that the viscous forces have very small contribution to the wave force acting on the porous cylinder and the solid column. Meanwhile, the effects of nonlinearities in the wave-structure interaction are relatively small.

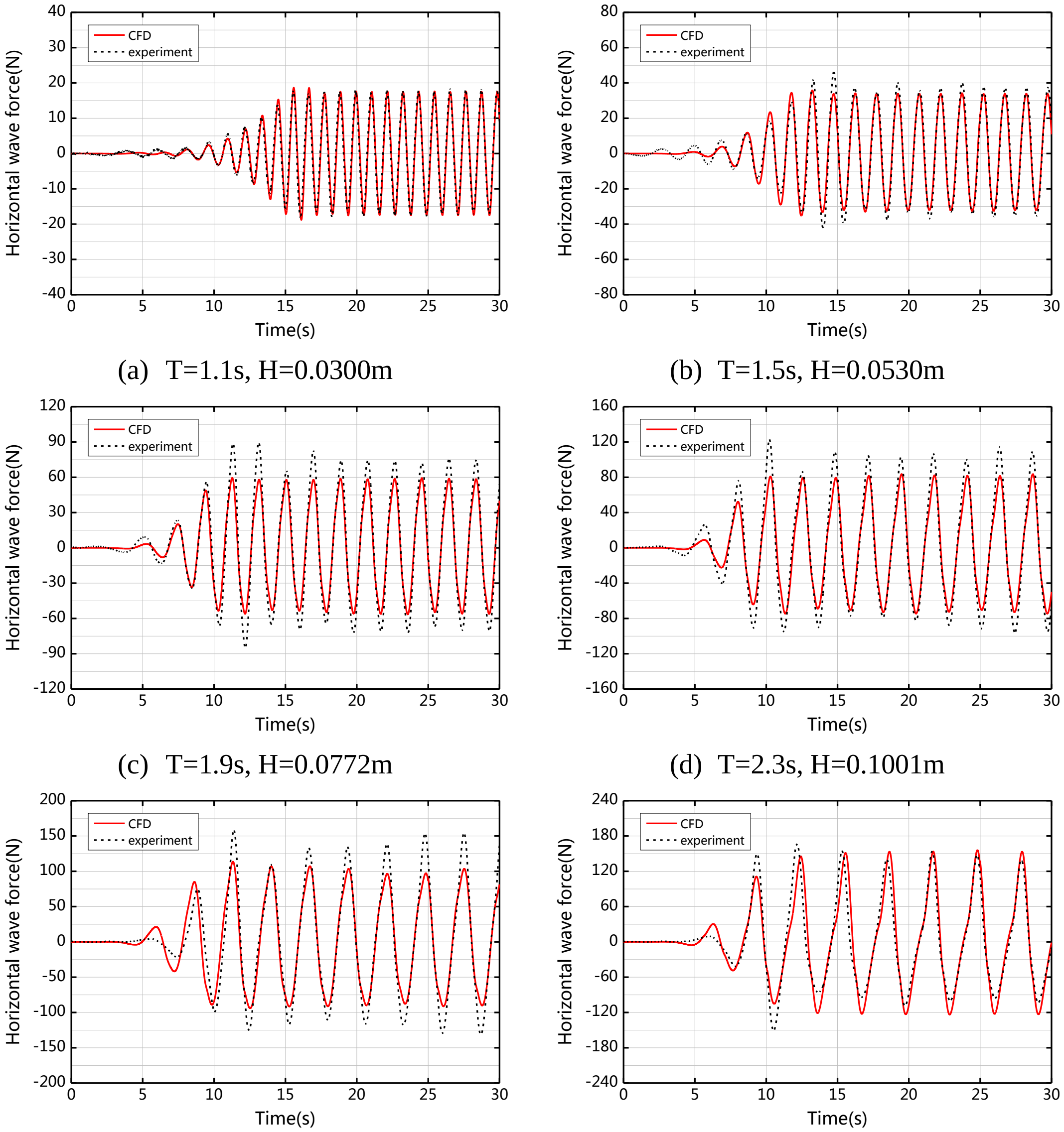

(a) T=1.1s, H=0.0300m
(b) T=1.5s, H=0.0530m
(c) T=1.9s, H=0.0772m
(d) T=2.3s, H=0.1001m
(e) T=2.7s, H=0.1221m
(f) T=3.1s, H=0.1437m

Figure 26 Time series of horizontal wave force on the combined cylindrical structure

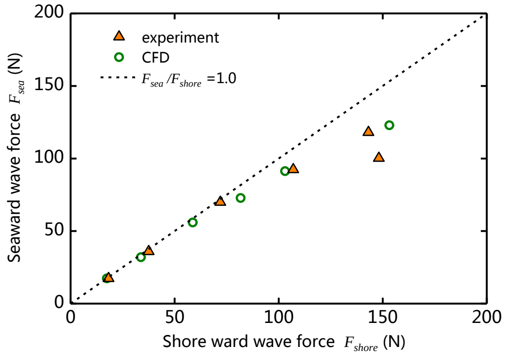

Figure 27 Seaward wave force against shoreward wave force on the combined cylindrical structure

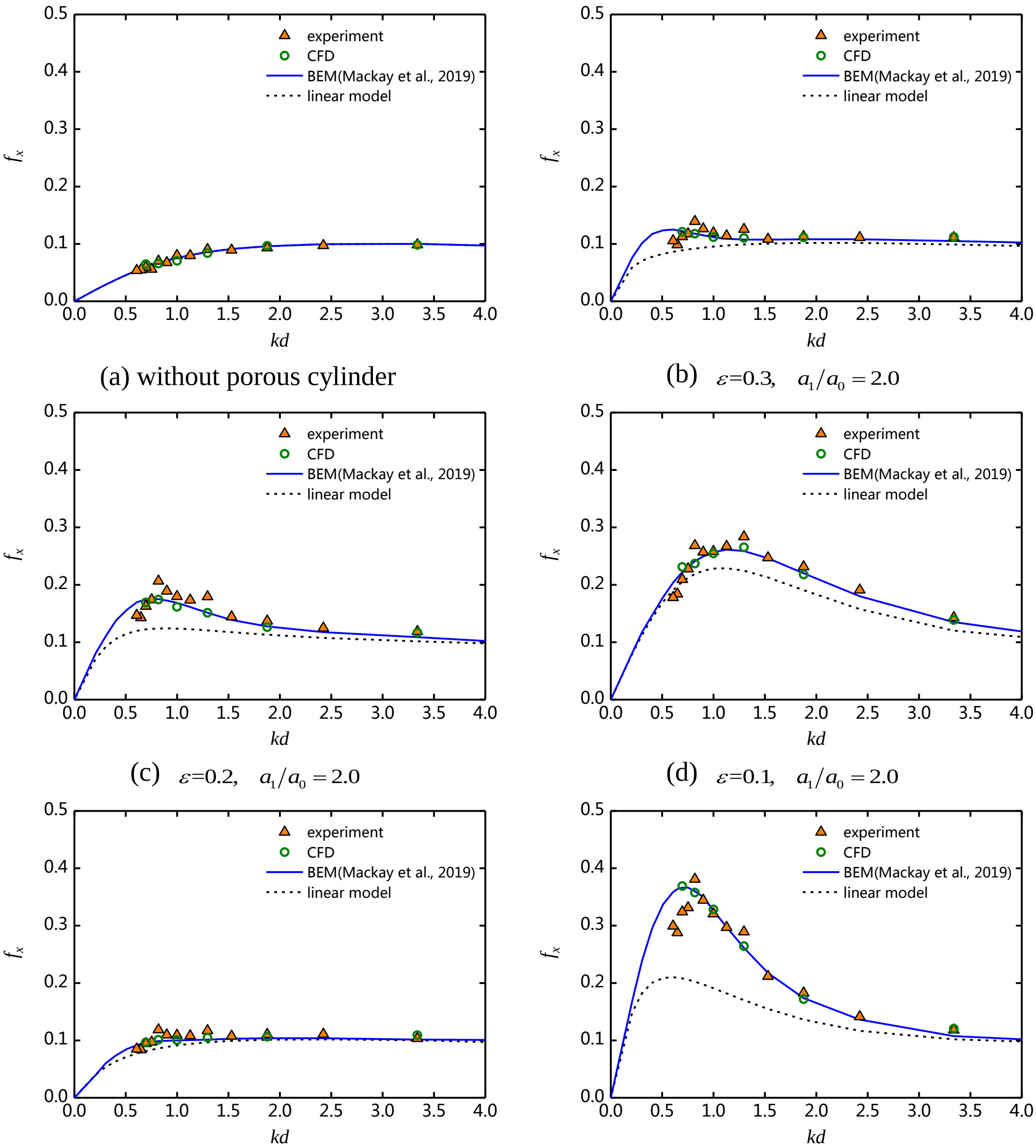

(a) without porous cylinder (b) ε=0.3, $a_1/a_0=2.0$

(c) ε=0.2, $a_1/a_0=2.0$ (d) ε=0.1, $a_1/a_0=2.0$

(e) ε=0.2, $a_1/a_0=1.5$ (f) ε=0.2, $a_1/a_0=3.0$

Figure 28 Normalized wave force on the combined cylindrical structure against *kd* with different geometrical parameters (kA=0.050, a_0=0.125m)

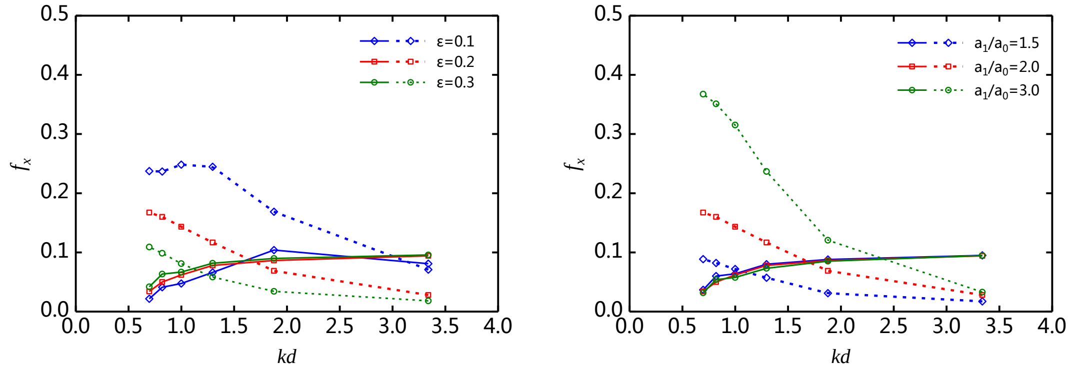

(a) (b)

Figure 29 Wave force on porous cylinder and inner column: (a) for wave force on porous cylinder and inner column of various porosity; (b) for wave force on porous cylinder and inner column various outer radii; solid lines for force on inner column and dash lines for force on porous cylinder

Figure 28(a)(b)(c)(d) show the comparison of the effects of porosity on the total wave force, where the radius of the porous cylinder shell is fixed as 0.50m and the porosities are 0.1, 0.2 and 0.3. It can be learned that the larger porosity is, the smaller wave force is, and the total wave force on the combined structure always larger than the case without a porous cylinder shell. Figure 29 shows the wave force on the inner column and outer porous cylinder. According to Figure 29(a), the variation of porosity has nearly no influence on the wave force on inner column. While the force on outer porous cylinder decreases with the porosity increasing, that is because the quadratic term of pressure-drop, which is the dominant component, decreases with the increasing of porosity. The effects of outer radius can be analyzed from Figure 28(a)(c)(e)(f), where the diameter of porous cylinder is 0.375m, 0.50m and 0.75m, the diameter of inner column is fixed as 0. 25m and the porosity is fixed as 0.2. It can be learned that the larger the outer radius is, the larger the wave force is, and the total wave force on the combined structure always larger than the case without a porous cylinder shell. According to Figure 29(b), the variation of outer radius has nearly no influence on the wave force on inner column. While the force on outer porous cylinder increases with the outer radius increasing, that is mainly because with the increasing of outer cylinder radius, the area of porous cylinder that wave acted on increases. For various parameters of porous cylinder, the total wave force increase very slightly for the cases of $\varepsilon=0.3, a_1/a_0=2.0$ and $\varepsilon=0.2, a_1/a_0=1.5$, which is the same as the case without a porous cylinder.

6 Wave force variation with wave amplitudes

In this section, a series of wave conditions with multiplied wave amplitudes and fixed wave frequency are applied to observe the variation of wave force on porous cylinder structures. The results are compared between experiments, present CFD method and the linear potential flow model, as shown in Figure 30. It can be observed from the experimental results that either for a single porous cylinder or a porous cylinder with a solid column, the normalized wave forces increase with kA, which means that the wave force increases at a greater rate than the multiplied increased wave amplitudes. The CFD results match well with experiments, illustrating that present CFD method can well replicated the increasing wave force with multiplied increased wave amplitudes. However, the linear potential model gives a constant line for normalized wave force with the increase of kA, meaning that the linear potential model predicts wave force increasing linearly with wave amplitudes. This is because the incident flow velocity is linearly related to the wave amplitude, while the wave force on porous cylinder is also linearly related to the pressure drop through the porous surface. Therefore, the relationship between the wave force and incident wave amplitude can be reflected by the pressure drop-velocity relationship. When the simplified linear pressure drop-velocity condition is adopted, the predicted wave force will be linearly related to the wave amplitude; when the pressure drop model gives pressure proportional to velocity squared, the predicted wave force will grow at a greater rate than the wave amplitude. The analysis above illustrates that the linear pressure drop model cannot replicate the wave force on porous cylinder structures increasing with wave amplitudes, and a quadratic pressure drop condition is more accurate for replicating this variation.

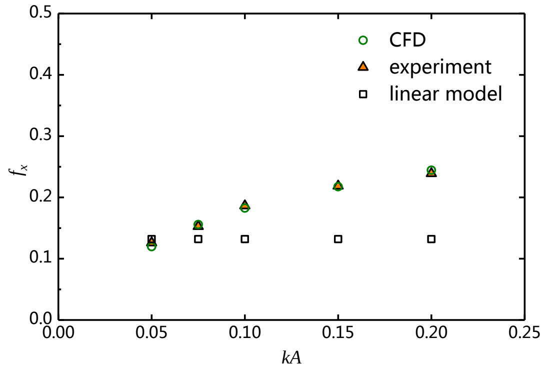

(a) For a single porous cylinder under T=1.5s (*kd*=1.88)

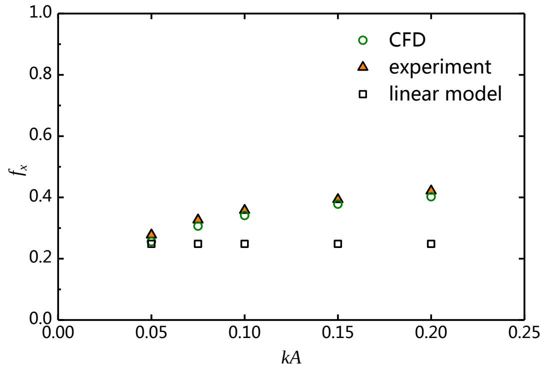

(b) For a single porous cylinder under T=1.9s (*kd*=1.30)

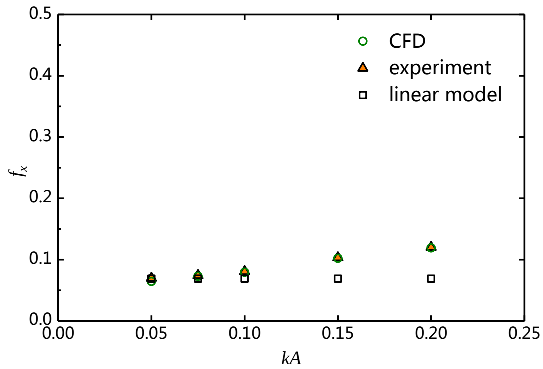

(c) For a porous cylinder with a solid inner column under T=1.5s (*kd*=1.88)

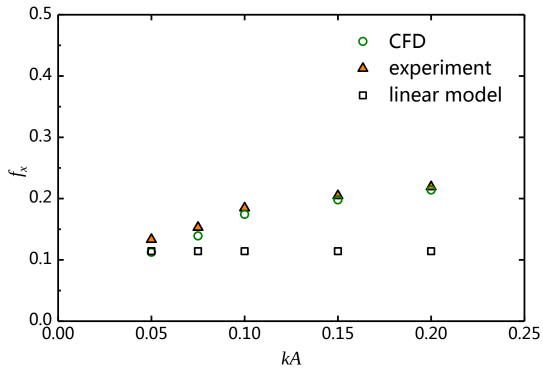

(d) For a porous cylinder with a solid inner column under T=1.9s (*kd*=1.30)

Figure 30 Variation of wave force on structures with multiplied increasing wave amplitudes (ε=0.2, $a_1/a_0 = 2.0$)

7 Conclusions

To investigate the wave interaction with fixed thin porous cylinders with and without inner impermeable columns, a numerical CFD model is established. The geometry of the porous cylinder is not resolved in detail but its effect on the flow is represented by a macro-scale model by means of a quadratic pressure drop and momentum source term, respectively. A series of corresponding tank tests were conducted as comparison. A linear potential model and a BEM model using quadratic pressure drop condition are also used for comparison and analysis. Following are several conclusions drawn in this paper:

(1) Through the comparison of experiments, present CFD method, a linear potential model and a quadratic BEM model, it can be learned that a linear pressure drop condition is not accurate enough to replicate the wave force, especially for low frequencies. On the contrast, the present CFD method and a BEM model both using a quadratic pressure drop condition can replicate wave force on porous cylinder well.

(2) Although the present CFD method has no obvious advantage on predicting wave force on porous cylinder compared to the existing BEM model, the meaning for the present CFD method is that it is fit for porous barriers with complex shape. It is also expected to solve the combined structures of porous barriers and solid bodies where the viscous force may be unable to be neglected, for example, when structures are in close proximity, or there is relative motion between them. Further investigation will be conducted based on present CFD method for these cases.

(3) The effects of geometrical parameters, porosity and outer cylinder radius, on wave force were analysis. The effects of porosity and outer cylinder radius on wave force were similar for the

two kinds of cylindrical structures. A larger porosity leads to a smaller wave force, and a smaller outer cylinder radius leads to a smaller wave force.

(4) For the free surface elevation inside the porous cylindrical structures, a smaller porosity leads to a smaller wave height inside, except for the backside interlayer of a porous cylinder with a solid inner column, where the wave heights were influenced significantly by backside reflection. An outer cylinder radius of $a_1/a_0 = 2.0$ and $a_1/a_0 = 3.0$ is deem to be effective for reducing wave heights inside porous cylindrical structures.

(5) The variation of wave force with multiplied increased wave amplitudes was analysed by comparing the results of experiments, present CFD method and the linear potential flow model. It is observed that the wave force on the two kinds of porous cylindrical structures increases at a greater rate than the wave amplitude. The linear pressure drop model cannot replicate this variation while the quadratic pressure drop correctly replicate this variation.

Acknowledgement

This work was supported by National Key R&D Program of China [Grant No. 2018YFB1501905], National Natural Science Foundation of China [Grant Nos. 51979030, 51761135011], EPSRC (UK) grant for the project 'Resilient Integrated-Coupled FOW platform design methodology (ResIn)'' [Grant No. EP/R007519/1], and Fundamental Research Funds for the Central Universities.

References

Bennett G. S., McIver P., Smallman J. V., 1992. A mathematical model of a slotted wavescreen breakwater, Coastal Engineering, 18 (3-4), 231-249.

Bonakdar, L., Oumeraci H., Etemad-Shahidi A., 2016. Run-up on vertical piles due to regular waves: Small-scale model tests and prediction formulae. Coastal Engineering, 118, 1-11.

Chen B., Wang L., Ning D., Johanning L., 2019. CFD Analysis on wave load mitigation effect of a perforated wall on offshore structure. Proceedings of the Twenty-ninth International Ocean and Polar Engineering Conference, Honolulu, Hawaii, USA, 3653-3658.

Chen H. and Christensen E. D., 2016. Investigations on the porous resistance coefficients for fishing net structures," Journal of Fluids and Structures, 65, 76–107.

Chen Q., Ma Y., Dong G., Ma X., Tai B., Niu X., 2020. A numerical investigation of interactions between extreme waves and a vertical cylinder. Journal of Hydrodynamics, 32(5), 853-864.

Christensen E. D., Bingham H. B., Skou Friis A. P., Larsen A.K., Jensen K.L., 2018. An experimental and numerical study of floating breakwaters. Coastal Engineering, 137, 43-58.

Chu Y. and Wang C., 2020. Design development of porous collar barrier for offshore floating fish cage against wave action, debris and predators. Aquacultural Engineering, 102137.

Chwang A. T., 1983. A porous wavemaker theory. Journal of Fluid Mechanics, 132, 395-406.

Cong P. and Liu Y., 2020. Local enhancements of the mean drift wave force on a vertical column shielded by an exterior thin porous shell. Journal of Marine Science and Engineering, 8, 349.

Darcy H., 18956. Les fontaines publiques de la ville de Dijon. Dalmont, Paris.

del Jesus M., Lara J. L., Losada I. J., 2012. Three-dimensional interaction of waves and porous structures. Part I: Numerical model formulation. Coastal Engineering, 64, 57-72.

Dokken J. S., Grue J., Karstensen L. P., 2017. Wave forces on porous geometries with linear and quadratic pressure-velocity relations. In: 32nd International Workshop on Water Waves and Floating Bodies, Dalian, China.

Feichtner A., Mackay E., Tabor G., Thies P. R., and Johanning L., 2021. Comparison of macro-scale porosity implementations for CFD modelling of wave interaction with thin porous structures. Journal of Marine Science and Engineering, 9, 150.
Feichtner A., Mackay E., Tabor G., Thies P. R., Johanning L., and Ning D., 2020. Using a porous-media approach for CFD modelling of wave interaction with thin perforated structures, Journal of Ocean Engineering and Marine Energy 1-23.
Feichtner A., Mackay E., Tabor, G., Thies P. & Johanning, L., 2019. Modelling wave interaction with thin porous structures using OpenFOAM, Proceedings of 13th European Wave and Tidal Energy Conference. Napoli, Italy.
Forcheimer P., 1901. Wasserbewegung durch Boden. Z. Ver. Dtsch. Ing, 45, 1782-1788.
Francis V., Ramakrishnan B., Rudman M., 2020. Experimental investigation on solitary wave interaction with vertical porous barriers. Journal of Offshore Mechanics and Arctic Engineering-transactions of the ASME, 142(4), 041205.
Gao L., Li J., 2012. Short-crested waves interaction with a concentric porous cylinder system with partially porous outer cylinder. China Ocean Engineering, 26.
Geng B., Wang R., Ning D., 2018. The wave absorption efficiency of multi-layer vertical perforated thin plates. Journal of Hydrodynamics, 30(5), 898-907.
Ha Y.-J., Kim K.-H., Nam B., Hong S.Y., 2020. Experimental investigation for characteristics of wave impact loads on a vertical cylinder in breaking waves. Ocean Engineering, 209, 107470.
Higuera P., Lara J. L., Losada I. J., 2014. Three-dimensional interaction of waves and porous coastal structures using OpenFOAM®. Part I: Formulation and validation. Coastal Engineering, 83, 243-258.
Huang Z., Li Y., Liu Y., 2011. Hydraulic performance and wave loadings of perforated/slotted coastal structures: A review. Ocean Engineering, 38(10), 1031-1053.
Jensen B., Jacobsen N. G., Christensen E. D., 2014. Investigations on the porous media equations and resistance coefficients for coastal structures. Coastal Engineering, 84, 56-72.
Liu H., Duan W., Chen X., 2013. Wave loading on concentric porous cylinders with varying porosity. Journal of Marine Science and Application, 12(4), 400-405.
Liu H., Zhang, L., Chen H., Zhang W., Liu M., 2018a. Wave diffraction by vertical cylinder with multiple concentric perforated walls. Ocean Engineering. 166, 242-252.
Liu J., Guo A., Nandasena N.A.K., Melville B., Li H., 2018b. Theoretical and experimental investigation on wave interaction with a concentric porous cylinder form of breakwater. Ocean Engineering. 160, 156-167.
Liu J., Zhong W., Shen K., 2013. Wave chamber of ultra large floating system. In: Proceedings of the 23rd International Offshore and Polar Engineering Conference. Anchorage, Alaska. ISOPE-I-13-115.
Liu P., Lin, P., Chang, K., Sakakiyama, T., 1999. Numerical Modeling of Wave Interaction with Porous Structures. Journal of Waterway, Port, Coastal, and Ocean Engineering, ASCE, 125:322-330.
Liu Y., Li J., 2017. Iterative multi-domain BEM solution for water wave reflection by perforated caisson breakwaters. Engineering Analysis with Boundary Elements, 77 (238), 70-80.
Liu Y., Yao Z., Xie L., 2012. Analysis of wave interaction with a submerged double layer horizontal porous plate breakwater. In: Proceedings of the Twenty-Second International Offshore and

Polar Engineering Conference. Rhodes, Greece.

Liu, Y., Li, Y., Teng, B., 2008a. Theoretical study of diagonal wave forces acting on partially perforated caisson breakwater with transverse walls. Acta Oceanologica, Sinica, 30(2), 137-146.

Liu, Y., Li, Y., Teng, B., Jiang J., Ma B., 2008b. Total horizontal and vertical forces of irregular waves on partially perforated caisson breakwaters. Coastal Engineering, 55(6), 537-552.

Mackay E, Liang H, Johanning L. 2021. A BEM model for wave forces on structures with thin porous elements. Journal of Fluids and Structures, 102(4): 103246.

Mackay E., 2020. Differences in wave forces on thin porous structures using linear and quadratic dissipation. 10.13140/RG.2.2.28984.37122.

Mackay E., Shi W., Qiao D., Roman G., Davey T., Ning D., Johanning L., 2020. Numerical and experimental modelling of wave interaction with fixed and floating porous cylinders. 10.13140/RG.2.2.16339.20002.

Mackay, E., Johanning, L., Qiao, D., Ning, D., 2019. Numerical and experimental modelling of wave loads on thin porous sheets. Proceedings of the 38th International Conference on Ocean, Offshore and Arctic Engineering, OMAE, 2019-95148.

McIver, P., 1998. The blockage coefficient for a rectangular duct containing a barrier with a circular aperture. Applied Ocean Research, 20, 173-178.

Metallinos A. S., Repousis E. G. and Memos C. D., 2016. Wave propagation over a submerged porous breakwater with steep slopes. Ocean Engineering, 111, 424-438.

Mohseni M., Esperança, P., Sphaier S., 2018. Numerical study of wave run-up on a fixed and vertical surface-piercing cylinder subjected to regular, non-breaking waves using OpenFOAM. Applied Ocean Research, 79, 228-252.

Molin B., 2011. Hydrodynamic modeling of perforated structures. Applied Ocean Research, 33(1), 1-11.

Molin B., Fourest J.M.,1992. Numerical modeling of progressive wave absorbers. In: proceedings of international workshop on water waves and floating bodies. Val de Reuil, France.

Molines, J., Bayón, A., Gómez-Martín, M. E., Medina, J. R., 2020. Numerical Study of Wave Forces on Crown Walls of Mound Breakwaters with Parapets. Journal of Marine Science and Engineering, 8(4), 276.

Neelamani S., Koether G., Schuettrumpf H., Muttray M., Oumeraci H., 2000. Wave forces on and water surface fluctuations around a vertical cylinder encircled by a perforated square caisson. Ocean Engineering, 27, 775-800.

Neelamani S., Uday Bhaskar N., Vijayalakshmi K., 2002. Wave forces on a seawater intake caisson. Ocean Engineering, 29, 1247-1263.

Ning D., Zhao X., Teng B., Johanning L., 2016. Wave diffraction from a truncated cylinder with an upper porous sidewall and an inner column. Ocean Engineering, 130, 471-481.

Polubarinova-Kochina, P., 1962. Theory of ground water movement. Princeton University Press, Princeton.

Qiao D., Feng C., Yan J., Liang H., Ning D., Li B., 2020. Numerical simulation and experimental analysis of wave interaction with a porous plate. Ocean Engineering, 218, 108106.

Ren X. and Ma Y., 2015. Numerical simulations for nonlinear waves interaction with multiple perforated quasi-ellipse caissons. Mathematical Problems in Engineering Theory Methods & Applications, 895673.

Sankarbabu K., Sannasiraj S. A., Sundar V., 2007. Interaction of regular waves with a group of dual porous circular cylinders. Applied Ocean Research. 29, 180-190.

Sankarbabu K., Sannasiraj S. A., Sundar V., 2008. Hydrodynamic performance of a dual cylindrical caisson breakwater. Coastal Engineering, 55, 431-446.

Shim K., Klebert P. and Fredheim A., 2009. Numerical investigation of the flow through and around a net cage. Proceedings of International Conference on Offshore Mechanics and Arctic Engineering, Honolulu, HI, USA, 43444, 581–587.

Sollitt C. K. and Cross R. H., 1972. Wave Transmission through Porous Breakwaters. In: Proceedings of 13th Conference on Coastal Engineering, ASCE, 3, 1827-1846.

Song H., Tao L., 2007. Short-crested wave interaction with a concentric porous cylindrical structure. Applied Ocean Research. 29.

Suh, K.D., Park, J.K., Park, W.S., 2006. Wave reflection from partially perforated-wall caisson breakwater. Ocean Engineering. 33 (2), 264-280.

Tabet-Aoul E. H. and Lambert E., 2003. Tentative new formula for maximum horizontal wave pressures acting on perforated caisson. Journal of Waterway, Port, Coastal and Ocean Engineering, 129(1), 34-40.

Vijayalakshmi K., Neelamani S., Sundaravadivelu R., Murali K. 2007a. Wave runup on a concentric twin perforated circular cylinder. Ocean Engineering, 34(2), 327-336.

Vijayalakshmi K., Sundaravadivelu R., Murali K., Neelamani S., 2007b. An experimental study on regular wave loads on a perforated circular caisson and suction pipe configuration. The Journal of Ocean Technology, 2(2), 50-63.

Wang K-H., Ren X., 1994. Wave interaction with a concentric porous cylinder system. Ocean Engineering, 21, 343-360.

Weng Y., Xu X., Huang H., 2016. Interaction of cnoidal waves with an array of vertical concentric porous cylinders. Applied Ocean Research, 58, 21-36.

Williams A. N., Li W., Wang K., 2000. Water wave interaction with a floating porous cylinder. Ocean Engineering, 27, 1-28.

Wu J., and Chwang A. T., 2002. Wave diffraction by a vertical cylinder with a porous ring plate. Journal of Engineering Mechanics, 128(2), 164–171.

Yu X., 1995. Diffraction of water waves by porous breakwaters. Journal of Waterway Port Coastal Ocean Engineering, 121(6), 275-282.

Zhao Y., Bi C., Liu Y., Dong G., and Gui F., 2014. Numerical simulation of interaction between waves and net panel using porous media model. Engineering Applications of Computational Fluid Mechanics., 8, 116-126.

Zheng Y., Shen Y., You Y., Wu B., Rong L., 2005. Hydrodynamic properties of two vertical truncated cylinders in waves. Ocean Engineering, 32, 241-271.

Zhong Z., Wang K., 2006. Solitary wave interaction with a concentric porous cylinder system. Ocean Engineering, 33, 927-949.

Zhu S., Chwang A. T., 2001. Investigations on the reflection behaviour of a slotted seawall. Coastal Engineering, 43(2), 93–104.